REVIEW

Invited Contribution from Award Winners of the 21st National Electrochemistry Congress in 2023

Surface Structures and Properties of High-voltage $LiCoO_2$: Reviews and Prospects

Jian-Jun Fang [a,b,#], Yu-Hao Du [a,#], Zi-Jian Li [a,#], Wen-Guang Fan [a,*], Heng-Yu Ren [a], Hao-Cong Yi [a], Qing-He Zhao [a,*], Feng Pan [a,*]

[a] School of Advanced Materials, Peking University Shenzhen Graduate School Shenzhen, Guangdong province, 518055, China
[b] Qiantu Battery Technology Co. Ltd., Dongguan, Guangdong Province, 523808, China

Abstract

Nowadays, the development of high-voltage $LiCoO_2$ (lithium cobalt oxide, LCO) cathodes has attracted the widespread attention from both the academic and industry fields. Among the multiple concerns, researches on the surface issues would provide the most effective performance optimization pathway for the synthesis of high-voltage LCO. In this work, the issues of high-voltage LCO, including the phase transitions and crack formation, the oxygen redox related issues and side reactions, as well as the surface structure degradation, have been systematically reviewed. Then, we further clarify the surface modulations, and the interplay between the surface modulation and electrolyte tuning. Finally, we propose our prospects for developing the more advanced LCO cathodes, including the low-cost and high-quality manufacturing, designing suitable LCO cathodes in some extreme conditions (such as high-temperature, high-rate charging, low temperature, etc.), and achieving stabilized capacity release of about 220 $mAh \cdot g^{-1}$ of LCO, etc. We hope that this work can serve as a reference to promote the development and application of high-voltage LCO in future.

Keywords: Lithium cobalt oxide; Interface structures; Phase transition; Surface modulation; Cathode electrolyte interphase

1. Introduction

In the past 30 years, the Li-ion batteries (LIBs) with $LiCoO_2$ (lithium cobalt oxide, LCO) cathodes have dominated the application for the usage in 3C products, including the computer, communication, and consumer electronics, etc., mainly due to its favorable features of high compacted density, high Li^+/electron conductivity, and excellent cycle life and reliability. Nowadays, the reversible capacity of LCO in practical applications has been limited to around 180 $mAh \cdot g^{-1}$, which is much lower than the theoretical capacity of 274 $mAh \cdot g^{-1}$ [1,2]. To build better batteries with higher energy density, elevating the charge cut-off voltage is a promising approach to unlock its full potential. For instance, when charged to 4.6 V vs. Li/Li^+, the available discharge capacity reaches around 220 $mAh \cdot g^{-1}$ (850 $Wh \cdot kg^{-1}$) [3]. However, applying higher voltage poses significant challenges for LCO cathodes, including the detrimental phase transitions, oxygen redox, and electrode/electrolyte interface reactions, etc. The intrinsic relationship among these issues is complex and interactive, and understanding the reaction routes and mechanisms of these issues is vital for optimizing the LCO performances. In recent research, scholars have explored various strategies to enhance the overall

Received 21 December 2023; Received in revised form 26 January 2024; Accepted 26 January 2024
Available online 21 February 2024

Jian-Jun Fang, Yu-Hao Du, and Zi-Jian Li contribute equally to this work.
* Corresponding author, Wen-Guang Fan, Tel: (86-755)26612204, E-mail address: fanwg@pku.edu.cn.
* Corresponding author, Qing-He Zhao, Tel: (86-755)26612204, E-mail address: zhaoqh@pku.edu.cn.
* Corresponding author, Feng Pan, Tel: (86-755)26612204, E-mail address: panfeng@pkusz.edu.cn.

https://doi.org/10.61558/2993-074X.3445

performance of batteries with LCO cathodes [4,5]. However, they primarily focus on the structure and properties of LCO itself under high voltage conditions.

When the charging cut-off voltage exceeds 4.55 V, the irreversible phase transition from O3 phase to detrimental H1-3 phase occurs. Due to the significant lattice variation and mismatch between the two phases, this phase transition leads to obvious Co-O slab slippage, and promotes the formation of micro-cracks inside the LCO particles [6,7]. The fragmentation of LCO particles inevitably brings the electrolyte infiltration into the interior of LCO, triggering more interface side reactions and gas release, leading to the severe voltage attenuation. In addition, the surface instability is of critical importance at high voltages. Due to the overlap of Co3d and O2p orbitals, the lattice O redox becomes active under deep delithiation, and part of the lattice oxygen near the surface region can be released in the form of O_2, which aggravate the interface side reactions, resulting in more electrolyte decomposition, gas release, and Co dissolution. The O loss in the surface region further causes the structure collapse or the phase transition from layer to spinel or rock-salt (RS), which gains the interface resistance, and leads to a deteriorated Li^+ transport [8,9]. As the cycle proceeds, the degradation of structural integrity occurs progressively, especially in the surface region. Thus, the above issues exacerbate the LCO failure, and eventually result in the capacity decay.

To extend the cycle stability of LCO at high voltages, some optimization strategies have been proposed in recent years, including the element doping, surface modulation, and electrolyte design. Element doping notably tunes the basic physical properties of materials, however, it introduces some inactive elements into the LCO cathodes, which leads to the lowered capacity release, and cancels the advantages of high voltage [10,11]. Thus, the composition design of LCO requires a comprehensive consideration of cycle stability, rate performance, and capacity release, etc. Besides, utilizing the single crystalline LCO materials is regarded as a feasible way to enhance the cycle stability, however, it usually requires long-term high temperature sintering process, which causes the increase in manufacturing costs. Since the structure deterioration of LCO is usually originated from the surface, stabilizing the LCO surface is of vital importance for enhancing the cycle stability of LCO cathodes [12]. The surface degradation issues, including the cathode/electrolyte side reactions, formation of the cathode electrolyte interface (CEI) layer, surface O loss, Co dissolution, surface structure collapse, and various defects formation, etc., can be greatly optimized or reduced via introducing the surface modulation. Forming a robust CEI is critical for stabilizing the surface structure, which can be tune form both the LCO surface design aspects, and the electrolyte aspects [13]. The most significant role of this robust CEI is to completely isolate the active LCO from the electrolytes, which helps to stabilize the surface Co-O framework of LCO. The cations mixing in the non-optimized LCO may lead to irreversible phase transitions and the transition metal (TM) ions dissolution [14]. The free TM ions can catalyze harmful interfacial reactions, promoting the growth of unstable CEI. After cycles, the heterogeneous CEI may affect the lithiation and delithiation processes of LCO, causing uneven lattice expansion, ultimately resulting in the intragranular cracks [13]. During the charge and discharge processes, the dynamic formation and dissolution of CEI may also impact the stability of the CEI structure [15,16]. Besides, the CEI must be low resistance for fast Li^+ transport, and high electronic conductivity to prevent impedance growth between particles, mitigating power losses, and in turn, promoting the kinetic processes of ions [17,18]. Furthermore, the CEI also must be chemically stable enough with less fluctuation of composition upon cycle. The above goals can be achieved via regulating the surface coating compositions or the electrolyte compositions, which will be discussed in the following sections.

Herein, the structures and properties of high-voltage LCO are summarized. Firstly, we illustrate the failure mechanism of LCO upon high voltages, including the phase transition beyond 4.55 V, the formation of crack, the lattice oxygen redox, the structure collapse, and side reactions, etc. Secondly, we emphasize the significant roles of the surface modulations on optimizing the surface integrity, including surface coatings, the reinforcement of surface Co-O frameworks, and the effects of foreign elements, etc. Thirdly, we clarify the beneficial mechanisms of electrolyte tuning from both solvents and electrolyte addictive species. Fourthly, we summarize the multiple optimization strategies, which are more practical, and can provide some guidance for designing the next-generation LCO cathodes. Finally, we propose our prospects for developing the more advanced LCO cathodes, including the more advanced sintering process for low-cost and high-quality manufacturing, the exploration for designing suitable LCO cathodes in some extreme service conditions (such as high temperature, high rate charging, low temperature, etc.), and achieving

stabilized capacity release of about 220 $mAh \cdot g^{-1}$ of LCO cathodes, etc. We hope that this work can serve as a reference to promote the development and application of high-voltage LCO in both the academia and industry.

2. Failure mechanism

$LiCoO_2$ belongs to the hexagonal crystal system with the space group R-3m. It adopts a layered structure composed of CoO_2 layers and Li layers stacked alternately. Within the CoO_2 layers, Co ions form a six-coordinated octahedral structure, while Li^+ ions are situated in the interlayer spaces of the layered structure. In ambient air conditions, the surface oxygen atoms of LCO are typically stable when exposed to the surroundings. During the charging process, the following reaction occurs:

$$LiCoO_2 \rightarrow Li_{1-x}CoO_2 + xLi^+ + xe^- \quad (1)$$

where Li^+ ions migrate from the positive electrode to the negative electrode. This process is often accompanied by an increase in the oxidation states of surface O and Co, especially at high voltages. In the discharging process, Li^+ ions can migrate back to the positive electrode, and the reaction is represented as

$$Li_{1-x}CoO_2 + xLi^+ + xe^- \rightarrow LiCoO_2 \quad (2)$$

Throughout the charge-discharge cycling, a solid electrolyte interface (SEI) layer accumulates on the surface of LCO. The CEI layer predominantly contains decomposition products of the electrolyte, effectively insulating LCO from direct contact with the electrolyte.

The structure failure of LCO upon high voltages distributes from the bulk to the surface of LCO particles, and the surface failure is usually more severe than that in the bulk. Typically, the failure forms include mainly the crack formation and the surface structure degradation. The formation of crack is mainly due to the large internal stress originated from the detrimental O3/H1-3/O1 phase transitions beyond 4.55 V (vs. Li/Li^+), and the uneven distribution of the state of charge (SOC) across the whole LCO particles upon cycles [19]. The surface structure degradation is basically attributed to the Co dissolution and O loss from the surface, which leads to the increased interfacial impedance. The side reaction can promote the Co dissolution from the surface, which in turn accelerates the structure collapse process.

At high voltages, there exists a close interplay among various issues in LCO, where the internal stress induced by the phase transition process is directly associated with the formation of cracks. The oxygen reduction-oxidation reaction leads to the release of surface oxygen, and Co dissolution resulting from surface side reactions induces degradation in surface structure, thereby promoting the initiation and propagation of cracks. Additionally, electrolyte decomposition side reactions form a CEI on the surface of LCO, increasing interface impedance and further exacerbating the electrochemical performance degradation of LCO.

In general, the application of LCO beyond 4.6 V faces the above complicated issues, and the combination and interaction of the issues promote the structure failure of LCO [19,20]. Understanding the failure mechanism is crucial for seeking suitable optimization strategies, which is the focus of this work.

2.1. Phase transitions and cracks formation

As the Li^+ ions are gradually removed from Li_xCoO_2, a progressive structure evolution occurs, as shown in Fig. 1a. In the region of $0.45 < x < 1$, the structure evolution contains a solid solution reaction process, with three first-order phases transformations. Further removing Li^+ ions from Li_xCoO_2 ($x < 0.45$) causes phase transitions from O3 to H1-3 and to O1 phases. The H1-3 phase has been confirmed to be a hybrid of the O1 and O3 phases structures [20]. As the structure evolves from the O3 to H1-3, the Co-O slabs shift along with the Li^+ rearrangement occurs, leading to the internal stress generation and structure damage. The shift of CoO_6 slabs upon the delithiation process of $LiCoO_2$ has been confirmed to be a collective and quasi-continuous migration process over a wide range of charge/discharge before the "Layer to Rocksalt" phase transition (Fig. 1b) [21]. The stripe-shaped O1 phase in the grain boundaries has been confirmed upon voltages over 4.7 V, acting as the main reason for the irreversible structural changes [22]. In addition, upon high voltage operation, the diffusion coefficient of Li^+ ions in LCO lattice can be regulated via tuning the Li/Co ratio of the pristine LCO and elemental doping [23,24].

The phase transition behaviors above 4.55 V bring very drastic changes in lattice volume, which causes significant anisotropic dimensional changes, and yields some mechanical fractures, such as lattice disorder, Li/Co antisites, oxygen vacancies, and microcracks, etc. These mechanical fractures gradually evolve into large voids and cracks across the LCO particles as the internal stress accumulates after long-term cycles. Two kinds of cracks are confirmed upon high voltage

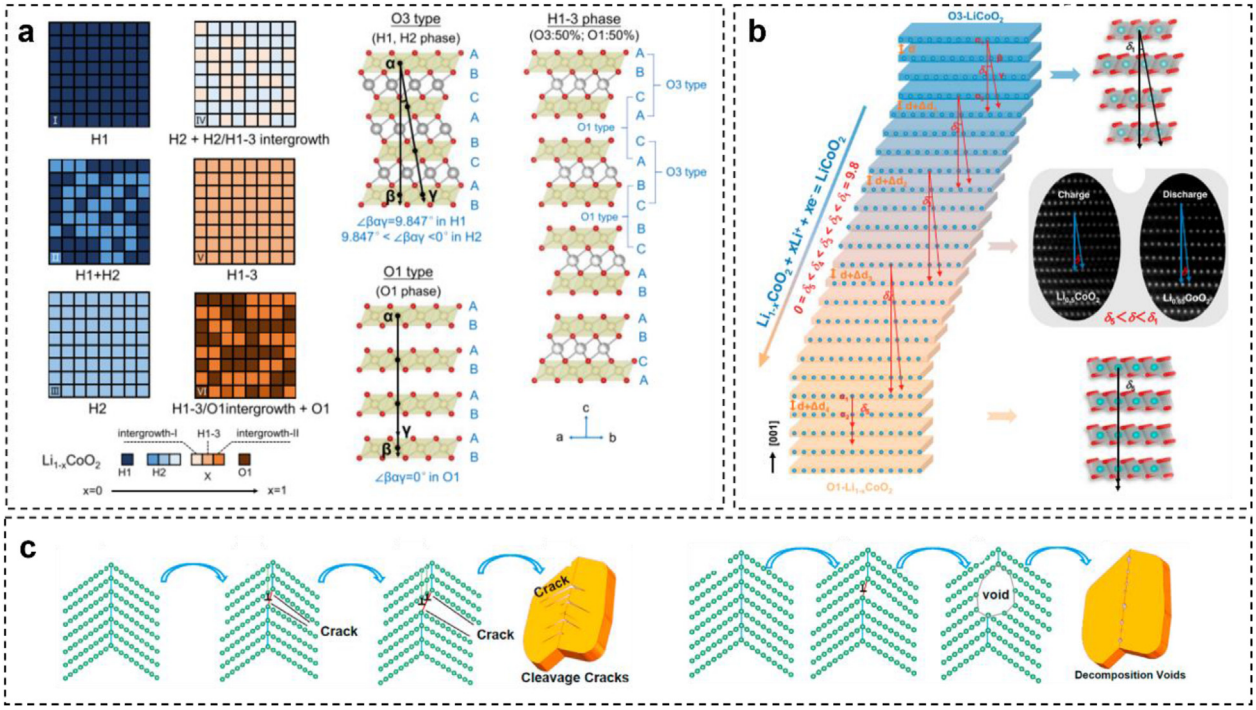

Fig. 1. (a) Diagram of LCO structure distribution during the entire phase transition process. Reproduced with permission [20]. Copyright 2023, ACS. (b) Collective glide of CoO_6 slabs in $Li_{1-x}CoO_2$. Reproduced with permission [21]. Copyright 2022, PNAS. (c) Nucleation and propagation of cleavage cracks and decomposition cracks. Reproduced with permission [25]. Copyright 2020, Elsevier.

cycling of LCO, including the cleavage crack and the decomposition crack (Fig. 1c) [25]. The former is a typical deformation induced mechanical failure, while the latter is formed due to thermodynamic decomposition, acting as the main cracking nucleation form upon high voltage cycle. As the cycle proceeds, the electrolyte will penetrate into the interior of LCO particles along these cracks and voids, which can induce more side reactions, and leads to the loss of active materials and the increase in charge transfer impedance. Therefore, the bulk structure degradation is one of the important reasons for capacity loss upon cycles. To break through the voltage limit of 4.55 V, it is crucial to suppress the detrimental structural changes upon cycle.

There are multiple factors which affect the nucleation and growth of cracks inside the LCO particles, including the internal lattice stress, the LCO particle size, the charge/discharge rates, the charging procedures, as well as the lattice defects, etc. The above influence factors play a significant role on affecting the cycle stability of LCO, mainly via modulating the homogeneity of phase transitions, especially upon a high voltage of >4.55 V, which promotes the formation of O3 and O3/H1-3 phase transitions. Kim et al. reported the substantial role of internal lattice strain on the oxygen release, lattice amorphization, and the subsequent crack formation, and they also demonstrated the energetically favorable formation of oxygen vacancies under shear strain (Fig. 2a) [26]. Jena et al. revealed the substantial differences in cycle performances of LCO cathodes with average particle distributions of 8 μm (LCO-A) and 11 μm (LCO-B) (Fig. 2b) [27,28]. They found that, for LCO-A, it followed a purely solid solution reaction during cycling, rather than the solid solution and two-phase reaction mechanism in LCO-B. As a result, the distribution of Li throughout the LCO-A particle was more homogeneous than that in LCO-B, leading to a more stabilized particle integrity, as well as the reduced crack formation. The influence of particle size on crack generation is more pronounced when operated under high voltage. Hitt et al. conducted the nanotomographic observation and statistical analysis of the overcharging induced cracks inside the LCO single crystalline particles [29]. They observed a strong particle size dependence on both nucleation and growth of cracks, specifically, the percentage of cracked particles, crack size, and crack surface area per unit volume, all increasing significantly with the increased particle sizes. A crucial fact is that the larger LCO particles contain more and larger cracks, mainly due to the increases in the pre-existing defects and energy release rate from crack advancement in larger particles.

The charging/discharging rates also present a significant impact on the high-voltage structure

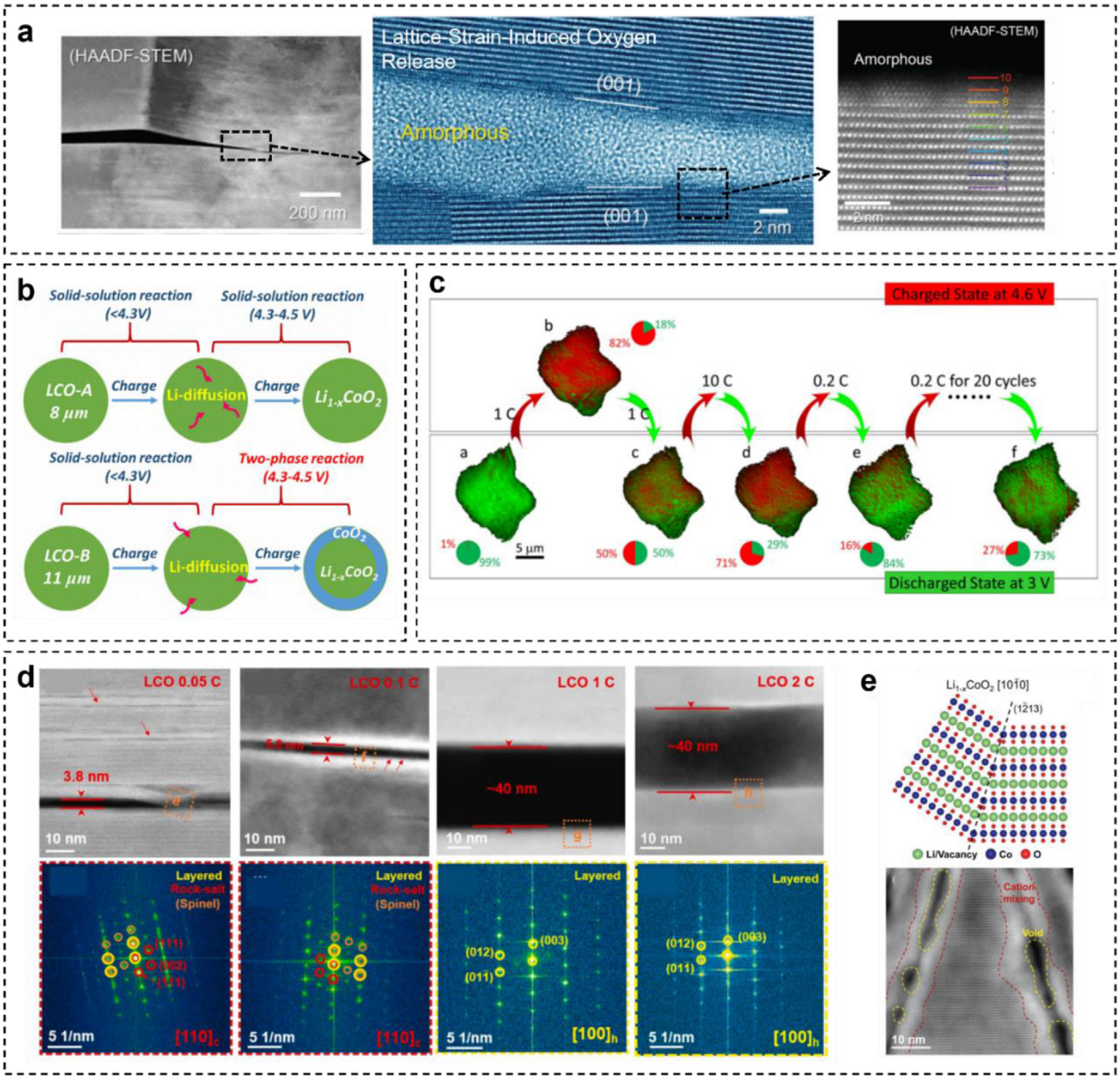

Fig. 2. (a) Lattice-strain-induced oxygen release and crack formation. Reproduced with permission [26]. Copyright 2023, Wiley. (b) Delithiation mechanism of LCO with different particle sizes. Reproduced with permission [36]. Copyright 2019, Wiley. (c) The in-situ monitoring of the chemical heterogeneity in a single LCO particle. Reproduced with permission [30]. Copyright 20117, ACS. (d) High-resolution TEM analysis on crack areas of LCO. Reproduced with permission [31]. Copyright 2023, Elsevier. (e) Twin-like grain boundary of the wedge-shaped crack. Reproduced with permission [32]. Copyright 2022, Wiley.

stability of LCO. Generally, the high charging/discharging rates tend to decrease the homogeneity of Li^+-ion's distribution inside the LCO particles, causing great internal stress to promote the crack formation. Xu et al. reported the uneven Li distribution and evolution of inactive domains in a single LCO particle upon cycles (Fig. 2c) [30]. They found that the evolution of the inactive regions inside the LCO is closely related to the cycling rate, and increasing the cycle rate could cause serious morphological degradation and the chemical inhomogeneity, thus leading to serious capacity decay. A better design of LCO requires conformal coating to prevent the Co dissolution and to realize homogeneous delithiation. Zhu et al. conducted a microscopic investigation of the crack and strain of LCO cathode cycled under high voltage (Fig. 2d) [31]. They demonstrated that, the fast charging could induce large cracks which can evolve into particle fractures, and the regions near cracks still retained a layered structure, while operated at low-rate charging, the generation of micro-cracks was observed, around which the irreversible phase transformation to rock-salt phases took place

through the Li/Co antisite and O loss. Besides, the crack formation is also affected by the lattice defects inside LCO. Oh et al. reported that the phase inhomogeneity of LCO could provoke the crack formation due to the stress relaxation (Fig. 2e) [32]. For an overcharged LCO, numerous voids in the crack boundary were observed after the crack formation, which acted as a path for electrolyte permeation, as well as the degradation of LCO structures. Yaqoob et al. revealed that, the formation of oxygen vacancy could be a reason for the crack formation in LCO [33]. They found that, the oxygen vacancy could introduce about 3% local stress-strain, which is much higher than the pure electrochemically-induced stress-strain, and is responsible for the crack formation. Besides, they also revealed that the formation of oxygen vacancy became more favourable with Li^+ extraction by exceeding 50%.

2.2. *Oxygen redox related issues and side reactions*

The lattice O oxidation (O^{2-} to $O^{\alpha-}$, $0 < \alpha < 2$) contributes capacity of LCO at voltages beyond 4.3 V. He et al. reported that, the electron localization function around the lattice O kept increasing upon delithiation, and it was increased significantly after more than 62.5% delithiation (Fig. 3a) [34]. This result indicated that the lattice oxygen participates in the charge compensation upon high voltage charging, and it became the main contributor to the charge compensation at a high delithiated state comparing with Co. Hu et al. concluded that, the oxygen redox took place globally inside the LCO, rather than just forming localized O−O dimerization [35]. They found that, the O−O pair distance was considerably shortened in the highly delithiated LCO, and no O−O bonds were formed in $LiCoO_2$ (Fig. 3b), which was very different from the lithium-rich system with formation of O−O bonds. The results toughly identified the possibility of applying highly reversible O redox to achieve high energy density of LCO cathodes. Further, Geng et al. performed the *ex-situ* ^{17}O NMR experiments to monitor the evolution of local O environments in LCO upon charging [36]. They revealed that, the O3(I)-O3(II) phase transition was driven by the electron delocalization within the Co-O layer, with the increased covalency of Co−O bonds, and the local lattice O environments were not uniform in the O3(III) and H1-3 phases with existence of a few local domains.

Owing to the overlap of O^{2-} 2p and $Co^{3+}/^{4+}$ 3d electronic bands, a deep delithiation triggers the lattice O oxidation, which causes the O release from the surface lattice of LCO [3,6]. Specifically, the Li^+ extraction from LCO leads to the increase of hole density in O 2p orbitals. Due to the reduced ionic radius and electrostatic force, $O^{\alpha-}$ has higher mobility than O^{2-}, which can move from bulk to the surface and release on the interface. The O release contributes to a series of cascading effects,

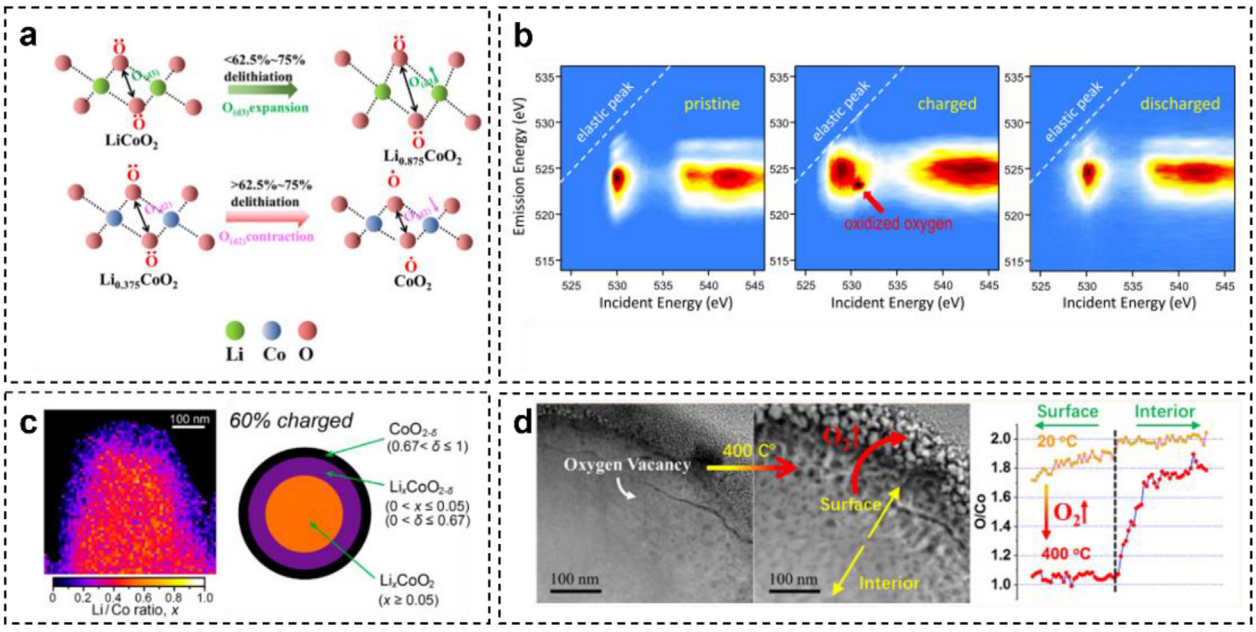

Fig. 3. (a) The O-O interlayer distance across the Li layer upon different delithiation states. Reproduced with permission [34]. Copyright 2023, RSC. (b) mRIXS of ex-situ $LiCoO_2$. Reproduced with permission [35]. Copyright 2021, Elsevier. (c) Quantitative maps of the Li/Co ratio in the charged $LixCoO_2$. Reproduced with permission [44]. Copyright 2015, ACS. (d) Thermal behavior of the high-voltage-cycled $LiCoO_2$. Reproduced with permission [39]. Copyright 2020, ACS.

including promoting the electrolyte decomposition, forming thick CEI layer, promoting phase transition from layer to the spinel, and even the rock-salt phases [36,37]. Accompanying with the surface O release, some Co^{2+} ions can be dissolved into the electrolyte, which brings terrible catalytic impact to compel more side reactions between the electrode and electrolyte.

The lattice O release is one of the main causes for the surface structural decay of LCO, and reducing the O release from the surface lattice of LCO is the key in developing the more advanced LCO with high cycle durability. Kikkawa et al. observed the overcharging induced Co^{3+}/Co^{2+} reduction with oxygen extraction from the LCO particle surface to the interior (Fig. 3c), with the presences of Co_3O_4-like and CoO-like phases at the surface regions after charging of 60% delithiation [36]. Hu et al. revealed the dynamic correlations between the Co ion migration and the oxygen dimer formation, and found that the formation of Co vacancy cluster is the prerequisite for the oxygen dimer generation [38], and the Ti doping could significantly reduce the Co migration and thus suppress the formation of Co vacancy cluster. Chung's team reported that, the oxygen release took place not only at the crystal surface but even inside the crystals [26]. DFT calculation results revealed that, the oxygen-vacancy formation value did not vary considerably under the compressive and tensile strains, while it became negative when the shear strain along the (001) plane basal was above a critical degree for LCO. That is to say, the LCO lattice with the substantial shear strain was energetically favorable for the formation of oxygen vacancies. Sun et al. reported a novel LCO degradation via oxygen vacancy facilitated Co migration and reduction, which leaves the undercoordinated oxygen and gave rise to the O release (Fig. 3d) [39]. This kind of LCO degradation is dominated by the kinetics of Co ions migration, and is closely related to the high voltage cycling defects in the LCO surface. Nowadays, although there existed a controversy on "whether it was the O loss promoted by Co migration, or the Co migration promoted by O loss", the close relationship between the O loss and Co migration and even dissolution was toughly confirmed. Therefore, stabilizing the lattice O was an important consideration in the design of high-voltage LCO cathodes.

The occurrence of O loss can further promote the side reactions, including the electrolyte decomposition and the formation of cathode electrolyte interface (CEI). Lu et al. reported that the formation of CEI layer was observed at the $LiCoO_2$ edge plane, not at the basal plane (Fig. 4a) [40]. Further, they revealed that applying the Al_2O_3 coating layer can improve the high voltage cycle stability of LCO via completely suppressing the formation of CEI at the edge planes. Rinke et al. reported that, the chemical oxidation (with an onset voltage of 4.7 V vs. Li/Li^+ for LCO) dominated the electrolyte decomposition process on the LCO surface, rather than the electrochemical reaction [41]. The reason can be ascribed to the reactive oxygen release at higher states-of-charge (SOC) of LCO, indicating that the reactions of the electrolyte on LCO surface are intrinsically linked to surface reactivity of the active material. Thus, regulating the interface chemistry of LCO materials can be an effective strategy to enhance the stability of high voltage cycling performance.

2.3. Surface degradation

For LCO cathodes charging over 4.55 V, not only the interface electrolyte decomposition aggravates rapidly due to the highly oxidative Co^{4+} and O^- on the LCO surface, but also the severe surface structure decay along with O loss and Co dissolution propagates from the surfaces into cores of LCO particles, leading to the dramatic capacity degradation. The previous report of our team revealed that, the curvature of the Co-O layers occurring near the surface dictated the structural stability of LCO cathodes at high potentials (Fig. 5a) [42]. Specifically, upon charging, the LCO had a larger layer curvature due to the removal of Li^+ ions, which continuously deteriorated and introduced higher structural stress and oxygen loss. These structure degradation in turn caused the aggravated layer curvature and further layer breakage, structure collapse and crystal fragmentation, which are more serious in the near-surface region. The curvature of Co-O layers is directly generated by the layer-stacking disorder from the possible mixed stacking modes, CoO_6 distortion and/or imperfect crystal growth, which could be by the crystal growth kinetics during synthesis.

It was reported that, the irreversible phase domain regions became larger as increasing the cycling voltage and cycle numbers. Takamatsu et al. reported that, the surface Co^{3+} is reduced to Co^{2+} immediately as long as the LCO contacts with the electrolytes [43]. Charging to a high voltage intensified the local distortions at surface of LCO, which propagated to the interior subsequently upon cycles. Besides, the severe O loss and Co dissolution from the LCO surface further promote the local structure damage and even form corrosion cavities at surfaces. Kikkawa et al. noticed that, the high voltage charging process can lead to

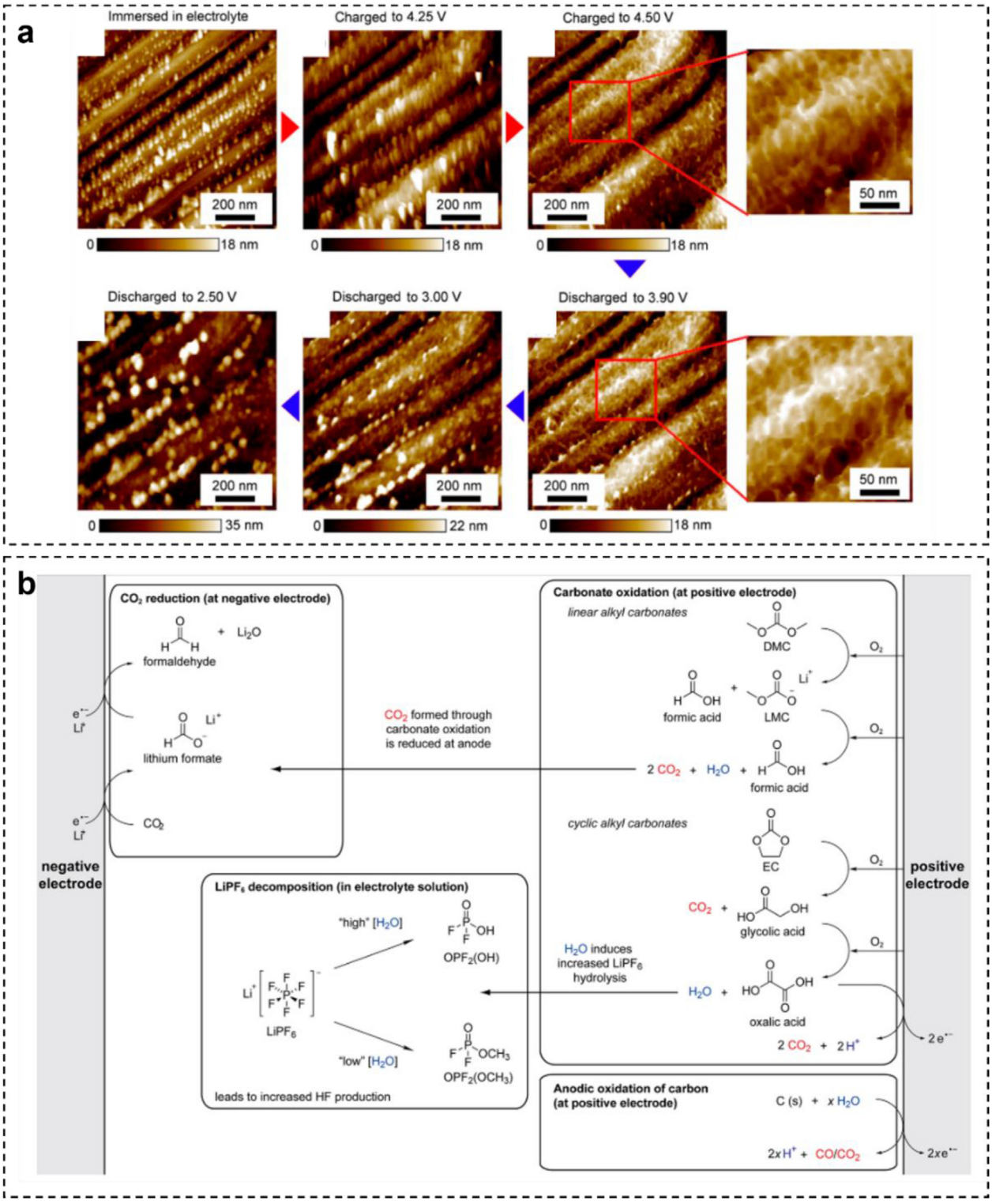

Fig. 4. (a) AFM images of in-situ monitoring of the CEI film formation and decomposition on the edge plane of $LiCoO_2$ crystal. Reproduced with permission [40]. Copyright 2017, ACS. (b) The electrolyte decomposition reactions that occur at high voltages (or high SOC) initiated at the positive electrode. Reproduced with permission [41]. Copyright 2020, ACS.

the inhomogeneous Li/Co distribution and Li-poor phase formation at the surface [44]. These Li-poor phases contained the CoO phase and Li-inserted Co_3O_4. Qin et al. studied the structural and chemical properties of the surface phase transition layer of LCO cycled at a cut-off voltage of 4.7 V (Fig. 5b) [45]. Structurally, the surface presents a spinel-like structure and contains high density of corrosion pits. Chemically, the LCO surface suffers substantial losses of O and Li, resulting in the Co

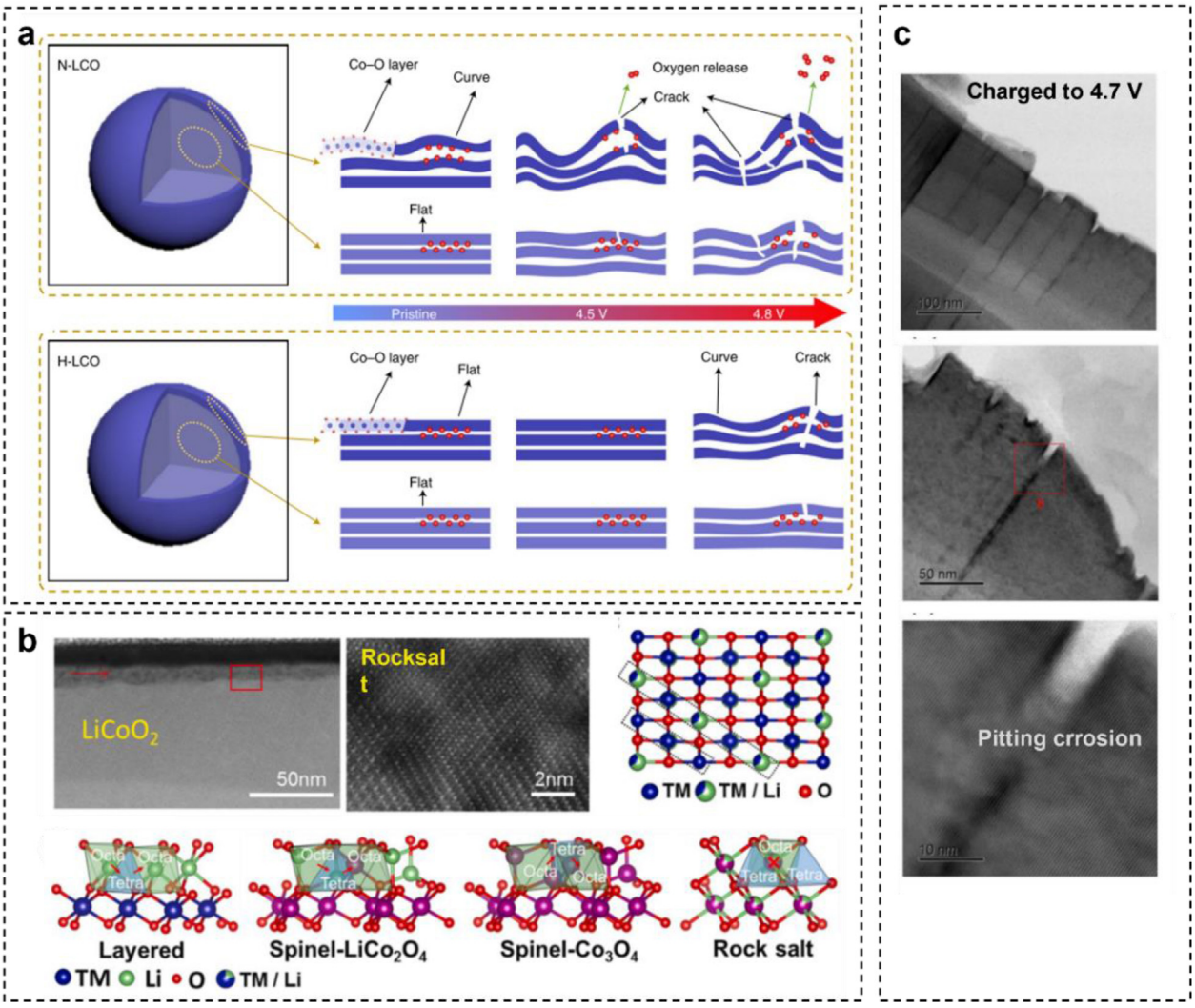

Fig. 5. (a) Schematic illustration of the LCO structural evolutions during charge. Reproduced with permission [42]. Copyright 2021, Nature. (b) A typical surface phase transition layer on surface of LCO. Reproduced with permission [45]. Copyright 2020, Elsevier. (c) The surface pitting corrosion of LCO charged to 4.7 V. Reproduced with permission [46]. Copyright 2017, ECSJ.

valence reduction, migration, and dissolution. They found that, the surface phase transition layer featured porous morphology and the spinel-like structure displays a negligible blocking effect on Li^+ ion diffusion, thus leading to the capacity decay. Yano et al. also reported the similar results of pitting corrosion on LCO surface upon high voltage of 4.7 V (Fig. 5c) [46]. They reported the occurrence of pitting corrosion and the formation of spinel-like layer on the surface of the cycled bare LCO. The pitting corrosion caused intrinsic capacity fading by Co dissolution, and the formation of the spinel-like layer resulted in the capacity decay due to the increased polarization. Furthermore, both the pitting corrosion and the formation of the spinel-like layer could be markedly suppressed by the surface coating.

Seong et al. systematically studied the intrinsic reversibility of LCO beyond 4.6 V, and concluded that the continuous formation of spinel phase surface layer was the main cause for the rapid capacity decay of LCO [47]. Notably, the spinel phase surface layer displays poor stability and can be easily etched as charging to 4.8 V. Lu et al. revealed that, the deep delithiation could induce some Co migrating to Li sites, leading to the formation of some incomplete rock-salt phase [48]. They also reported that, in the highly delithiated $LiCoO_2$, the unique charge compensation process leads to a spatial charge gradient of $Co^{2+}/Co^{3+}/Co^{4+}$ ions from surface to bulk, which can be further manipulated by the structural distortion, Li^+ extraction, and surface side reactions. Hirooka et al. examined the LCO degradation upon floating charge process in LCO/Graphite cells (45 °C and 4.4 V) [49] and concluded that: (1) the HF generated by the decomposition of $LiPF_6$ reacts with the charged $LiCoO_2$ electrode, (2) the charged $LiCoO_2$ electrode is disproportionated

into CoO_2 and Co^{2+} ions, and (3) the CoO_2 with an O1 structure is decomposed into cobalt oxides containing cobalt ions in a lower oxidation state, accompanying with the oxygen gas evolution. Yan's group [50] reveals that the exposed surface facets can significantly influence the surface stability. Specifically, the surface facets perpendicular to the (002) planes suffer more severe cracking and corrosion, while other surface facets are much more stable. The surface facets oblique to the layered-planes are intrinsically more resistant to mechanical cracking and chemical corrosion due to the modulated stress release by transition metal condensation.

The formation of CEI layer also plays significant roles on the capacity decay of LCO. Aurbach et al. investigated the surface chemistry of LCO upon different voltages and temperatures [50]. Comparing with the bulk structure destruction, the LCO surface degradation might play more significant roles on the capacity decay of LCO, and the surface chemistry of LCO could be to tuned with electrolyte additives that are decomposed on the electrode surfaces (e.g., polymerization) to form stable and steady CEI layers. Zhang et al. performed a quantitative analysis on the CEI layers on both LCO cathode and Li anode [51]. They found that, the evolution of CEI layer was mainly due to the continuous reactions of electrolyte and physical migration of SEI fragments from the lithium anode. For LCO/graphite cells, the CEI layer on LCO surface was not significantly changed because of the relatively stable SEI layer formed on the graphite anode. Yan et al. further reported the retarding effect of CEI layer of LCO on the transportation of Li^+ ions upon high voltage [22]. The decomposition of organic electrolytes and the formation of CEI became inevitable as charging over 4.5 V, and achieving a high-performance CEI layers with high stability and ionic conductivity was very important for the enhanced cycle stability of LCO cathodes.

3. Surface modulation

Surface modification is regarded as an effective approach to enhance the electrochemical performance of LCO. It enables the optimization of the surface structure of LCO, leading to the formation of a protective layer that resists the corrosion from HF, suppresses Co dissolution, and inhibits O release. Besides, a well-engineered surface structure can also facilitate the surface ion transport, thereby enhancing reaction kinetics. The exploration of surface modulations has been massively reported, including the surface coatings with oxides or solid electrolytes, the polyanion's modulations, as well as the reinforced surface Co-O frameworks with spinel or RS phases. Table S1 compares the electrochemical performance improvement promoted by various surface modulations for LCO. The following section is the detailed discussion to address these iuuses.

3.1. Surface coating with oxides or solid electrolytes

In the initial stages, lots of attempts have been made to form simple coating layers using oxides or solid electrolytes. Cho et al. employed the sol-gel method to initially coat Al_2O_3 on LCO, forming a $LiCo_{1-y}Al_yO_2$ solid solution on the surface (Fig. 6a). This enables LCO to exhibit a capacity of 174 $mAh \cdot g^{-1}$ at 4.4 V and 0.5 C conditions, maintaining 97% capacity after 50 cycles [52,53]. Based on this result, Feng et al. has successfully achieved a capacity of 180 $mAh \cdot g^{-1}$ at 4.5 V and 0.5 C with 73% capacity retention after 500 cycles, by controlling the thickness of the Al_2O_3 coating layer [54]. MgO is also commonly used for surface coating of LCO. Huang et al. has coated a layer of MgO on commercial lithium cobalt oxide, achieving stable cycling at 4.3 V/4.5 V and obtaining a capacity of 210 $mAh \cdot g^{-1}$ at 4.7 V and 0.1 $mA \cdot cm^{-2}$ [55]. Currently, it has been widely believed that the mechanisms of action for Al_2O_3 and MgO are similar. On one hand, they serve as protective layers to stabilize the surface structure (Fig. 6b), and on the other hand, during cycling, the diffusion of Al^{3+}/Mg^{2+} into the lattice of LCO acts as a support (Fig. 6c) [56−59]. In addition to Al_2O_3 and MgO, extensive explorations have been conducted on other oxides. ZnO has a hexagonal structure similar to LCO [60], with alternating layers occupied by Zn and O atoms, facilitating the ZnO epitaxial growing on the surface of LCO. Furthermore, ZnO doped with elements such as Al and Ga exhibit excellent electronic conductivity [61], which is beneficial for improving the rate performance of LCO. Gao et al. utilized the sol-gel method to coat Al-doped ZnO on the surface of LCO, achieving 98.2% capacity retention after 50 cycles at 4.5 V and 0.5 C, along with a reversible capacity of 156 $mAh \cdot g^{-1}$ at 8 C [62]. TiO_2 possesses good structural and thermal stabilities, and can react with HF to form a more stable and conductive interface layer containing TiF_x, significantly improving the electrode performance of LCO. Li et al. has directly sputtered TiO_2 on surface of LCO, and the prepared LCO electrode maintained 86.5% capacity after 100 cycles at 4.5 V and 1 C [63]. Despite the above benefit effects, most metal

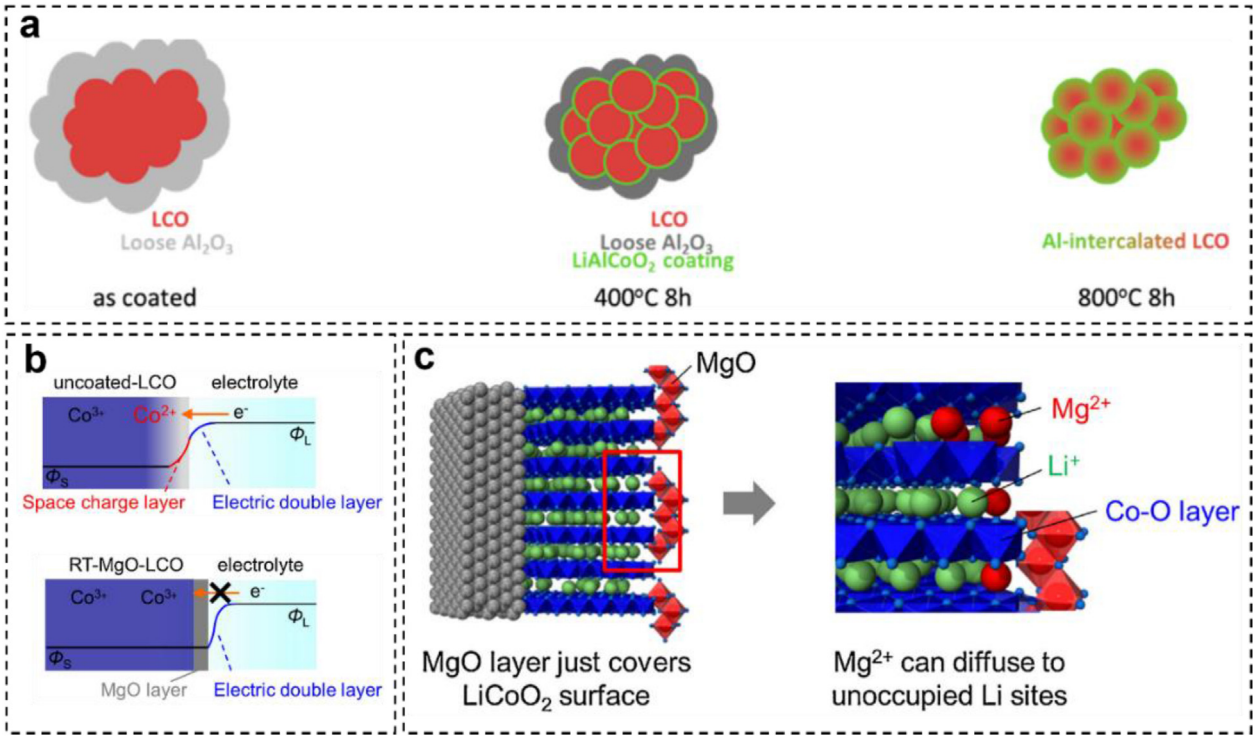

Fig. 6. (a) Schematic diagram of the interaction between Al_2O_3 and LCO. Reproduced with permission [58]. Copyright 2017, ACS. (b) Schematic diagram illustrating the effect of MgO coating on LCO surface. Reproduced with permission [57]. Copyright 2014, ECSJ. (c) Schematic diagram illustrating the supporting role of Mg^{2+} occupying Li sites [57]. Copyright 2014, ECSJ.

oxides are not good Li^+-ion conductors, which may hinder the transmission of Li^+ ions during cycling, thereby affecting the electrode performance. Therefore, the use of solid electrolyte coatings which is capable of rapid Li^+ conduction has been developed, such as $Li_{1+x}Al_xTi_{2-x}(PO_4)_3$ (LATP). Chen et al. has prepared an ultra-thin LATP coating on the surface of LCO using a solution method, achieving 93.2% capacity retention after 50 cycles at 4.5 V and 0.2 C [64]. Yang et al. has replaced Ti in LATP with Ge, and prepared the electrode by ball milling, which maintained 88% capacity after 400 cycles at 4.5 V and 1 C [65].

3.2. Surface modulations with inert anions

Although the surface modulations with oxides or solid electrolytes can improve the cycle stability to some extent, the benefit effect is not sufficient at more higher voltages, such as 4.6 V. As the voltage requirements for LCO continue to rise, when the voltage reaches 4.6 V, LCO undergoes a more destructive O3 to H1-3 phase transition, accompanied by complicated phase transitions and numerous surface side reactions, leading to the irreversible surface structure degradation and unlimited CEI growth. The serious Co and O losses can reduce the amount of Li^+ storage sites and hinder the transport of Li^+ ions, resulting in the rapid capacity decay. Therefore, simply using oxides or solid electrolytes for surface modification is not able to resist capacity decay at 4.6 V [1,3].

In order to achieve stable cycling of LCO at high voltages, researchers have initiated efforts via introducing some inert elements such as F, P, B, Se, S, etc., to achieve better surface modifications. LiF, for instance, can stabilize the surface of LCO with F without introducing additional elements (Fig. 7a) [66]. Lu et al. have constructed a three-layer structure containing F on the surface of LCO, namely, a surface LiF layer, a transition layer, and a gradient-doped layer with F, having a total thickness of approximately 100 nm. This structure can act as a physical barrier, stabilizing lattice oxygen, while establishing a robust and complete Li^+ transport pathway. They have achieved a capacity retention of 82.5% after 100 cycles at 4.6 V and 0.5 C, mainly attributing to the reduced Li^+ migration energy and the stabilization of lattice oxygen by F [67]. Aurbach et al. utilized a hydrothermal method to form a protective Li-Al-F coating on the surface of LCO, effectively suppressing the irreversible O3 to H1-3 phase transition. The electrode exhibited a capacity retention of over 78% after 500 cycles at 4.6 V and 0.5 C [68].

Phosphorus (P) can help to form phosphates on surface of LCO, exhibiting excellent Li^+ conductivity and chemical stability. Once the strong

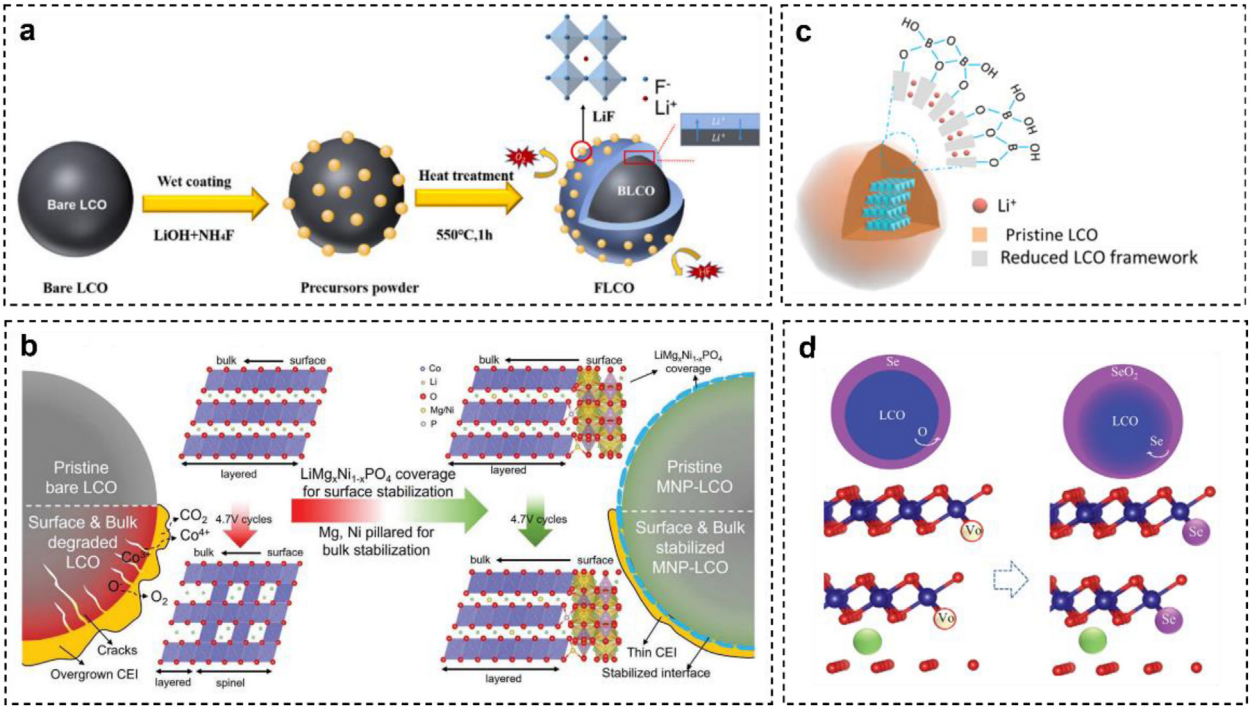

Fig. 7. (a) LCO surface coated with a corrosion resistant LiF layer. Reproduced with permission [66]. Copyright 2022, Elsevier. (b) Schematic diagram illustrating the combined effect of surface phosphate coating and Mg/Ni doping [72]. Copyright 2023, Wiley. (c) Schematic diagram illustrating the interaction between B and the surface of LCO [74]. Copyright 2021, ACS. (d) Se replacing oxygen vacancies generated during the cycling process in LCO [76]. Copyright 2020, Wiley.

covalent P-O tetrahedron is formed at the interface, it can effectively reduce the surface oxygen activity of LCO, and suppress the oxygen release. Lu et al. have introduced 2% $Li_3Al(PO_4)_2$ on the surface of LCO, and the capacity retention values of 88.6% and 78.6% were obtained at 30 °C and 45 °C, respectively, after 200 cycles at 4.6 V and 0.5 C. They attributed the enhanced performance to the crucial role of Li_3PO_4, which can effectively improve the mobility of Li^+ ions [69]. Huang et al. has designed a $Zr_3(PO_4)_4$ coating layer, effectively enhancing the electrode performance of LCO in the temperature range of −25 °C−25 °C. The electrode maintained 91% capacity retention after 300 cycles at −25 °C, 4.6 V and 1C [70]. Yang et al. have epitaxially grown a lattice-matched LiCoPO4 layer outside the LCO lattice, and the strong P−O bond significantly reduces the surface oxygen activity. The electrode maintained 87% capacity after 300 cycles at 4.6 V and 1 C, and operated stably at 4.6 V/55 °C and 4.7 V/30 °C [71]. Furthermore, researchers have explored the combination of surface phosphate modification and element doping to enhance the electrode performance of LCO. Cheng et al. have utilized $LiMg_xNi_{1-x}PO_4$ for surface modification with Mg and Ni doping, achieving 78% capacity retention after 200 cycles at 4.7 V and 0.5 C. They suggested that the Mg/Ni can occupy the Li sites to inhibit the harmful O3/H1-3 phase transition, and the $LiMg_xNi_{1-x}PO_4$ contributes to the formation of a uniform and stable CEI (Fig. 7b). Moreover, the strong covalent bond between P and surface oxygen can further improve the electrode performance [72]. Huang et al. have designed a super wettable LCO with shallow surface Zr doping and surface $Li_2Zr(PO_4)_2$ modification, which achieves a 94% capacity retention after 100 cycles at −25 °C, 4.6 V and 1 C. The Zr doping agent plays a significant role on enhancing the crystal structure stability, promoting the Li^+ diffusion, and suppressing the lattice oxidation. Besides, the surface phosphate modification can facilitate the formation of a stable and highly Li^+ conductive CEI [73].

Boron (B) can also form strong B−O covalent bonds when combined with the lattice oxygen of LCO. Xiao et al. have introduced the $LiBH_4$ onto the surface of LCO using a wet chemistry method. The highly oxygen-affine B^{3+} is rapidly combined with the LCO surface, accompanying with the reduction of Co^{3+} (Fig. 7c). After the $LiBH_4$ modification, LCO maintained 95% and 85% of its capacity after 100 cycles at 4.6 V and 1 C, and 500 cycles at 5 C, respectively [74]. Ji et al. have introduced a Co_xB_y coating on the surface of LCO, combining with Mg doping, which achieves 94.6% capacity retention after 100 cycles at 4.6 V and 1 C. They proposed that the interface bonding effect between the Co_xB_y and

the LCO surface can enhance the formation energy of oxygen vacancies, thereby significantly reducing the lattice oxygen losses [75].

Selenium (Se) also exhibits strong interactions with O. Li et al. have used Se to replace some of the O on the surface of LCO, achieving a capacity retention of 77% after 550 cycles under full-cell conditions at 4.57 V and 100 $mA \cdot g^{-1}$. They proposed that, Se can capture the oxygen escaped from the LCO, and simultaneously, Se can substitute for some of the $O^{\alpha-}$ generated during the charging process, extracting its charge and reducing it back to O^{2-} (Fig. 7d) [76]. Zheng et al. have shared a similar perspective with Li, suggesting that Se can interact with O^{2-} 2p in the deep delithiation state. With the combination of Se coating and Mg doping, the LCO can achieve a capacity retention of 72.9% after 1000 cycles at 4.6 V and 1 C [77].

Compounds containing sulfur (S) have been commonly used in high nickel layered oxide cathodes. Previous studies have shown that S-containing species can convert surface residual lithium contaminants into Li_2SO_4. The stable Li_2SO_4 can act as a physical barrier, preventing direct contact between the cathode material and the electrolyte [78,79]. Zheng et al. have introduced the sulfur compounds into the LCO system. They used $Ti(SO_4)_2$ to interact with LCO, forming a Li_2SO_4 and $Li_2CoTi_3O_8$ coating layer on the surface of LCO. Under conditions of 4.6 V and 1 C, the obtained LCO electrode maintained 77.85% of its capacity after 100 cycles [80].

3.3. Reinforced surface Co-O framework

In the above mentioned studies, the surface of the modified LCO retains its layered structure. However, in some surface modifications, there may exist a transformation of the surface structure of LCO from the original layered phase to spinel or rock salt phases, mainly due to the doping of elements near the surface. Lu et al. have prepared a ternary lithium aluminum fluoride surface-modified LCO, and the coating layer exhibited a stable and conductive surface (Fig. 8a). The modified LCO showed a capacity retention of 81.8% after 200 cycles at 4.6 V and 27.4 $mA \cdot g^{-1}$. They observed that, in addition to the surface coating layer, a thin doping layer was formed near the surface of LCO, primarily consisting of Li-Al-Co-O-F solid

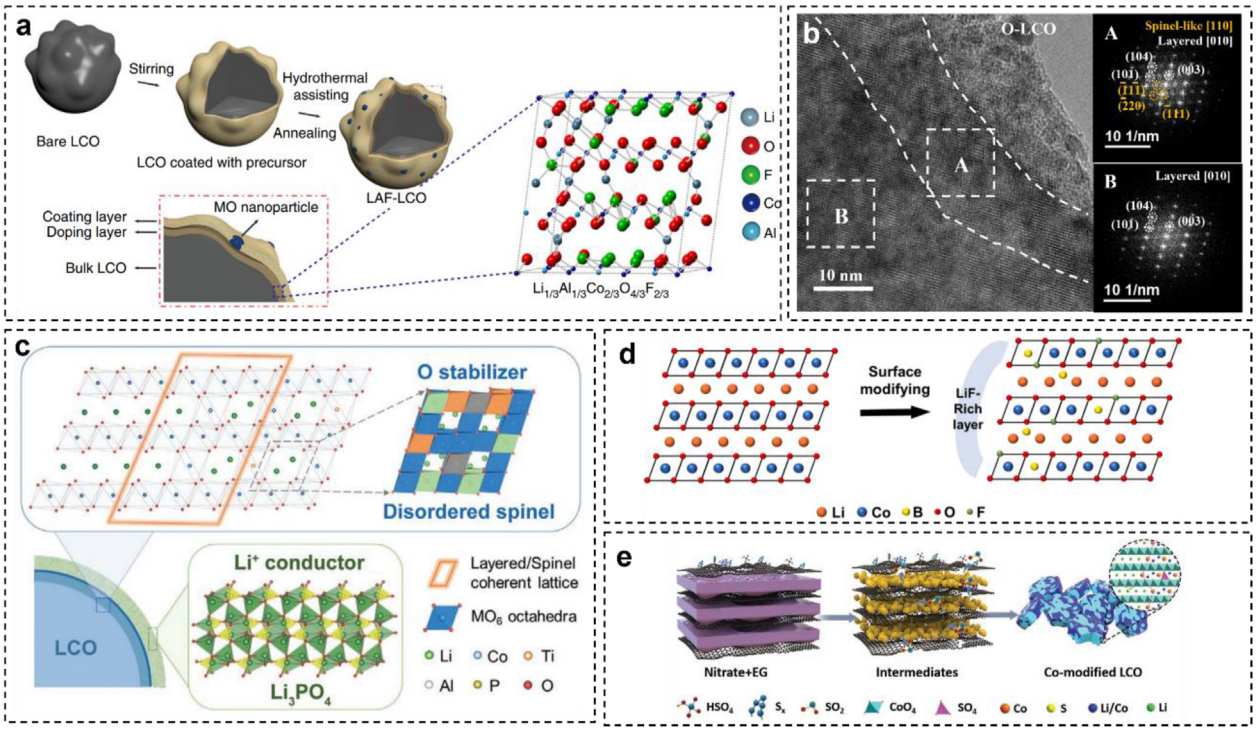

Fig. 8. (a) LAF surface modification of LCO, forming a thin doped layer near the surface. Reproduced with permission [81]. Copyright 2018, Nature. (b) TEM images of LAFP surface modification on LCO, forming a thin spinel-like layer near the surface. Reproduced with permission [82]. Copyright 2023, Wiley. (c) Schematic diagram of LCO with surface phosphate coating and a disordered spinel-like layer near the surface [83]. Copyright 2020, Wiley. (d) Schematic diagram illustrating the role of B in the lattice of LCO [85]. Copyright 2023, Elsevier. (e) Schematic diagram illustrating the role of sulfur-containing compounds in the lattice of LCO [87]. Copyright 2022, Wiley.

solution. They suggested that this layer can suppress the phase transition of LCO when the operating voltage exceeds 4.55 V [81]. Our research group further introduced P into the Li-Al-F system to modify the LCO. We observed the formation of a spinel phase in the subsurface (Fig. 8b), and believe that this spinel phase can contribute to the structural enhancement. The electrode achieved a capacity retention of 83.2% after 500 cycles at 4.65 V and 1 C and 74.6% after 500 cycles at 4.6 V and 1 C under a temperature of 45 °C [82].

Li et al. have introduced a complete spinel phase on the surface of LCO via a solid-state electrolyte coating of LATP, and a heat annealing strategy (Fig. 8c). Additionally, the Li_3PO_4 was generated in the outermost layer. They suggested that the oxidation ability of oxygen in the spinel phase lattice is much weaker than that in the layered structure, resulting in excellent high-temperature stability. The electrode achieved a capacity retention of 88.3% after 100 cycles at 4.6 V and 0.5 C, and after elevating the temperature to 45 °C, it maintained 72.9% after 100 cycles. This result represents a significant improvement of cycle stability comparing with the previous solid-state electrolyte coating [83]. Using a similar strategy, they have uniformly coated TiO_2 and $LiPO_2F_2$ on surface of LCO, and then followed by sintering to induce a reaction with LCO, leading to the *in-situ* formations of $LiCoTiO_4$ and Li_3PO_4. A transition of the LCO surface structure from layered to spinel has been observed, which achieves a capacity retention of 96.7% after 100 cycles at 4.6 V and 0.5 C [84].

Furthermore, Li et al. have constructed a LiF layer on the outer surface of LCO using $LiNO_3$, NaF, and H_3BO_3. Upon the above synthesis, a spinel structure with gradient doping of B and F near the surface of LCO was obtained. They considered that, B can occupy the Co sites (Fig. 8d), forming stable B−O bonds, and a small amount of B can enter into the interstitial sites to provide higher lattice stability. F can occupy the O sites, forming Co−F bonds with significant bond energy, stabilizing the lattice structure. Ultimately, they have achieved a capacity retention of 95.2% after 800 cycles at 4.6 V and 1 C [85]. Chu et al. have proposed an *in-situ* sulfur-assisted solid-phase method, utilizing the gas-solid interface reaction between metal oxides and sulfur to construct a gradient-doped surface of $Li_xCo_2O_4$ spinel and SO_4^{2-} polyanions on the surface of LCO (Fig. 8e). The electrode has achieved a capacity retention of 89.7% after 300 cycles at 4.6 V and 1 C [86]. Using a similar strategy, they have employed sulfur-containing expanded graphite as a template to prepare a surface with $Li_xCo_2O_4$ spinel and trace sulfur doping near the surface. The electrode achieved a capacity retention of 88% after 100 cycles at 4.6 V and 1 C [87].

4. Interplay between surface modulation and electrolyte tuning

The CEI is a layer formed on the LCO surface upon cycles, and it has been regarded as a crucial factor influencing the electrode reactions. A uniform, stable, and Li^+ conductive CEI is essential for stabilizing the cathode structure and ensuring the reversible Li^+ ions transport. The study about forming a qualified CEI can be approached from two perspectives: a) the CEI modulations from the LCO materials aspect; b) the in-situ construction of CEI via electrolyte tuning. Table S2 compares the electrochemical improved performance promoted by CEI modulations.

4.1. CEI modulations from the materials aspect

Firstly, from the material's aspect, electrolyte solvents such as EC, will undergo oxidation on the surface of LCO, forming organic-rich CEI at the charged state [88]. Although some researchers believe that the organic components have advantages in reducing the conduction impedance of Li^+ ions [13], the electrochemical stability of organic CEI is unsatisfactory. It tends to undergo repeated generation and dissolution during charging and discharging processes [51]. Therefore, the regulation of CEI needs to focus on the stability of CEI, which can effectively protect LCO [89]. From the material's aspect, researchers have optimized the CEI composition on surface of LCO generally using the following two strategies, a) the surface modification can affect the electrolyte decomposition pathway, and then influence the CEI film species; b) the *in-situ* transformation of surface coatings, i.e., transforming to new species which is favorable for enhancing the physicochemical properties of CEI.

For the first strategy, researchers mainly focus on the altered electrolyte decomposition process due to the surface modification. For example, Liu et al. have coated LCO with a layer of $Li_4Mn_5O_{12}$ (LMO) [90], which alters the adsorption species on the lithium-depleted LCO surface Hemlholtz layer (IHL) from EC to PF_6^-, and induces the formation of more LiF in the CEI layer (Fig. 9a). The resulting CEI, enriching in the inorganic LiF components, demonstrates superior stability, higher Young's modulus, and thermal stability. They also performed an *in-situ* heating TEM analysis of the CEI, and found that, the optimized CEI maintained a dense structure even heated to 500 °C. Wang et al.

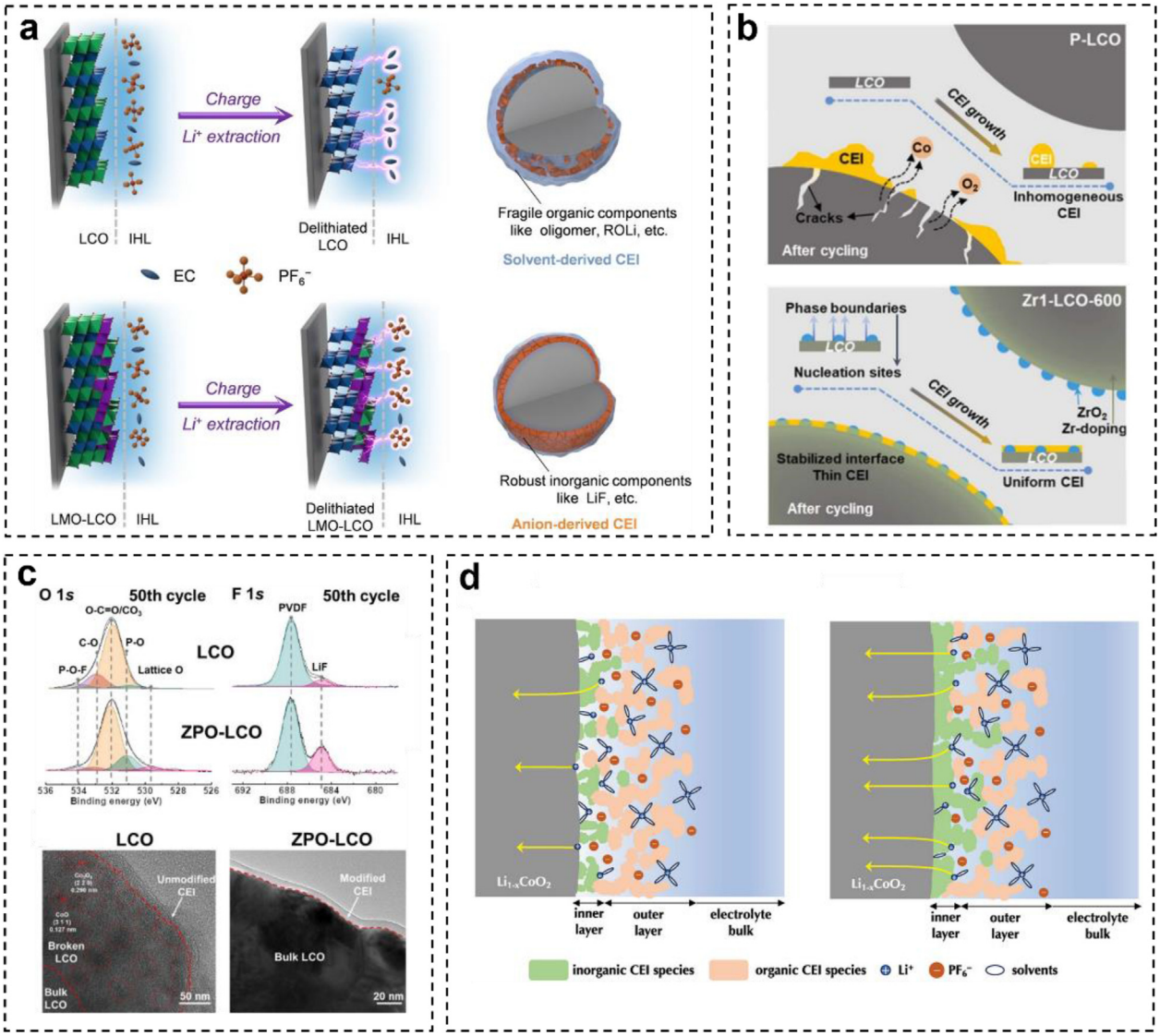

Fig. 9. (a) Passivation of the reactive cathode surface through spinel coating, achieving anion-derived IHL and LiF-rich CEI. Reproduced with permission [90]. Copyright 2022, Wiley. (b) ZrO_2 nano-rivets are constructed on the surface of LCO, providing phase boundaries for preferred film-forming sites, inducing the formation of uniform and robust CEI. Reproduced with permission [92]. Copyright 2023, Elsevier. (c) Surface amorphous $Zr_3(PO_4)_4$ achieves high-quality CEI with strong stability, good wettability, and high Li^+ conductivity. Reproduced with permission [70]. Copyright 2022, ACS. (d) The surface modification of Li_2ZrO_3 helps to form a dense CEI mainly composed of inorganic substances, which facilitates the rapid desolvation of lithium on CEI and achieves excellent rate capability. Reproduced with permission [94]. Copyright 2023, Wiley.

have designed LCO with Mg-rich surface and bulk doping of Al and Ti [91]. The Mg-rich surface layer stabilized CEI can suppress the decomposition of $LiPF_6$ into $Li_xF_yPO_z$, and enhance the electronic and ionic conductivities. Thus, it achieved a first discharge capacity of 224.9 $mAh \cdot g^{-1}$ at 3−4.6 V and retained 78% of capacity after 200 cycles. Zhuang et al. have designed LCO with $LiMg_xNi_{1-x}PO_4$ coatings, which reduces the decomposition of electrolyte carbonate solvents and alkyl lithium salt ($ROCO_2Li$), and inhibits the conversion of $LiPF_6$ to $Li_xPF_yO_z$ [72]. The $LiMg_xNi_{1-x}PO_4$ coating has been believed to help maintain the stability of CEI of LCO upon cycling. Even after 200 cycles at 4.7 V, it could still provide 78% reversible capacity. Zhang et al. have proposed that between the surface-dispersed ZrO_2 nano-rivets and LCO (Fig. 9b), there is a high interfacial energy, serving as the favorable nucleation sites for the uniform formation of CEI layer [92]. This continuous and dense CEI ensures an 80% capacity retention for LCO after 700 cycles at 4.6 V.

For the second strategy, researchers have focused on the *in-situ* conversion of surface coatings upon cycling, exploring how the derived Li^+ conductive species improve the CEI properties. For example, Ye et al. have coated LCO with a layer of uniformly distributed amorphous $Zr_3(PO_4)_4$ with a thickness of about 5 nm [70]. The amorphous $Zr_3(PO_4)_4$, after cycling, can facilitate the formation

of more inorganic components containing LiF and P−O bonds, resulting in the stable and low-impedance CEI (Fig. 9c). The optimized LCO displayed a capacity of 179.2 mAh·g^{-1} at −25 °C (0.2 C, 4.6 V) after cycling. Wang et al. have also investigated the role of P−O bonds in CEI, designing a coating layer on the surface of LCO using $Li_{1.5}Al_{0.5}Ti_{1.5}(PO_4)_3$ (LATP) [83]. After sintered at 700 °C, the coating formed olivine Li_3PO_4 phase and spinel (Co_3O_4, $CoAl_2O_4$, and Co_2TiO_4) on the LCO surface. This coating can regulate the CEI layer after cycling, inducing more LiF and Li_3PO_4 productions in CEI. The high conductivity and chemically stable Li_3PO_4 significantly reduces the CEI impedance, and shows high thermal stability. Wang et al. have designed an artificial CEI by a cross-linked structure obtaining from 3-aminopropyltriethoxysilane (APTES) on the surface of LCO [93]. This artificial CEI can strengthen the surface Co−O bonds, and reduce the oxygen release from the lattice. In contrast, bare LCO with shortened Co−O bonds upon charge can lead to the transition from O3 to O1. Zhou et al. have grown Li_2ZrO_3 layer on surface of LCO. The *in-situ* neutron reflectometry (NR) results showed that the electrolyte can fill the cavities in the CEI layer during the initial cycles (Fig. 9d) [94]. Li_2ZrO_3 can react with electrolyte substances and impurities like HF and H_3PO_4 in the cavities, generating LiF and Li_3PO_4, and forming a dense inorganic CEI. The high density CEI forces the Li^+ ions to undergo an desolvation process to diffuse to the inner layers through the solid-solid interface within CEI, which can accelerate the desolvation of Li^+ ions, resulting in the excellent rate performance (the average voltage exceeding 3.8 V at 100 C).

4.2. CEI modulations from the electrolyte aspect

From the perspective of regulating CEI properties, in addition to focusing on the material's aspect, the regulation of electrolytes cannot be ignored. Traditional carbonate-based electrolytes, such as EC, with a lower oxidation potential [95], tend to form a porous and unstable CEI layer when the voltage exceeds 4.3 V (vs. Li/Li^+) [96]. This unstable CEI layer undergoes repeated decomposition/regeneration during charge/discharge processes [9], causing continuous damage to the LCO surface. Additionally, the dehydrogenation reaction of EC-based electrolytes at high voltages triggers the decomposition of $LiPF_6$ into corrosive HF acid [97], further inducing damage to the LCO surface structure. Therefore, regulating electrolytes to suppress side reactions are crucial for the optimized interface chemistry, especially the construction of a protective CEI layer.

The previous strategies achieving stable CEI of LCO via electrolyte regulation mainly focus on the following aspects: a) adding low-potential decomposable additives to traditional carbonate-based electrolytes to inhibit continuous oxidative decomposition at high voltages or to preferentially form a robust CEI on LCO surface, effectively isolating the LCO from electrolyte, b) designing new electrolyte system using solvents with higher oxidation potentials than EC-based electrolytes to match the high-voltage LCO. Besides, the practical application of batteries also requires the design of novel wide-temperature-range electrolytes.

The presence of trace water in batteries is fatal because trace water provides hydrogen when LiPF6 is decomposed into HF acid [98]. The presence of HF accelerates the degradation of the LCO. Researchers, such as Bizuneh et al., have focused on the role of electrolyte additives on removing water [99]. They have reported the utilization of 4-nitrophthalic anhydride (NPA) to inhibit HF generation in electrolytes, and the $-NO_2$ groups on NPA can further introduce LiN_xO_y to the CEI on surface of LCO, which significantly reduces the CEI impedance. The dehydrogenation reaction of EC has been considered as the key factor in inducing HF production at high voltages [100]. Yan et al. effectively suppressed EC dehydrogenation by adding potassium (4-methylsulfonylphenyl) trifluoroborate (SPTF) in the traditional EC-based electrolytes [101]. They confirmed the inhibitory effect of SPTF on HF generation, and showed that the SPTF can affect the nature of the CEI on LCO surface. Compared to CEI formed with traditional EC-based electrolytes, the CEI assisted by SPTF had a thinner, higher Young's modulus, and more stable characteristics.

In addition to inducing HF acid, carbonate-based electrolytes, when in contact with highly delithiated LCO surface, tend to form Li^+-insulated CEI rich in organic fluorides as the main components [102], especially in the presence of PF_5 (a decomposition product of $LiPF_6$). Guo et al. have reported that the bis-(benzenesulfonyl) imide (BBSI) additive presents the highest binding energy with PF_5 under the influence of hydrogen bonding, resulting in the stabilized PF_5 and regulated CEI composition (Fig. 10a) [103]. Specifically, BBSI can be decomposed preferentially on the LCO surface, forming a CEI enriched with the Li^+-conductive components (Li_2S-rich, low-content LiF). The adsorptive $ROSO_2Li$ is considered to be beneficial for forming a dense CEI, thus inhibiting the reduction decomposition of carbonates [104].

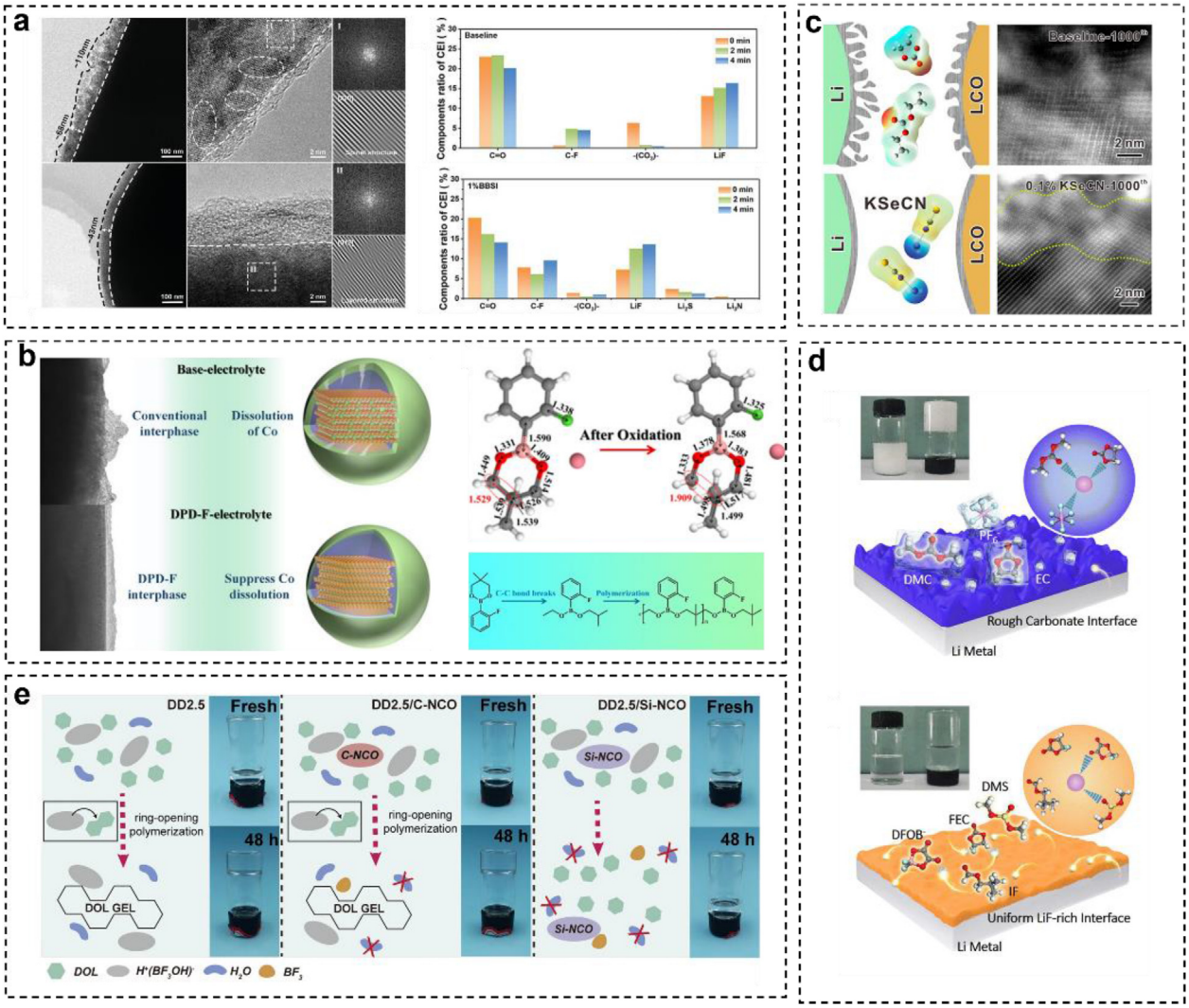

Fig. 10. (a) The BBSI additive constructed a uniform and high Li^+ conductive CEI on the surface of LCO. This CEI layer is composed of LiF and conductive Li^+ moieties (such as Li_2S and Li_3N), which can improve Li^+ migration. Reproduced with permission [103]. Copyright 2023, Wiley. (b) DPD-F constructs F- and B-rich CEI on the surface of LCO, inhibiting the dissolution of transition metal ions and nucleophilic reactions between the electrolyte and cathode. Reproduced with permission [106]. Copyright 2023, ACS. (c) A stable and dense SEI/CEI membrane constructed by adding trace KSeCN to traditional carbonate electrolytes through synergistic effects of -Se and -C≡N groups. Reproduced with permission [108]. Copyright 2023, ACS. (d) A fluorine sulfur electrolyte designed by using IF as an antifreeze to achieve low coordination number, high solvent removal energy. The formation of abundant F radicals can construct a stable LiF rich CEI layer. Reproduced with permission [111]. Copyright 2022, RSC. (e) The open-loop polymerization of DOL eliminates trace water in an electrolyte, ensuring that LCO has good low-temperature performance. The addition of Si-NCO promotes the formation of thin and inorganic rich CEI. Reproduced with permission [112]. Copyright 2023, Wiley.

Yang et al. have proposed that, the cyano group (−CN) preferably coordinates with Co^{4+} on the LCO surface, reducing the true valence of Co, and ultimately inhibiting the catalytic decomposition of high-valent Co in carbonate-based electrolytes [105]. The synergy of nitrile and FEC can regulate the morphology and chemical composition of CEI, forming a dense, thin, and LiF-containing electron-insulated CEI. The cells achieved 75% capacity retention after 300 cycles at 3−4.6 V, 30 °C, and 1 C, and 63% retention after 200 cycles at 55 °C. Sun et al. have reported that the 1-(5,5-Dimethyl-1,3,2-dioxaborinan-2-yl)-2-fluorobenzene (DPD-F) had a lower oxidation potential than carbonate solvents (EC, DMC, DEC), and could be preferentially decomposed to form a CEI film on LCO surface (Fig. 10b), which is dense, thin, and enriched with LiF-rich inorganic components and boron-rich organic components [106]. The function mechanism is as follows, i.e., upon oxidation, the C−C bonds in DPD-F break into radicals, following with spontaneous polymerization, forming a unique structure with an outer organic layer and an inner inorganic layer, which is beneficial to Li^+ conduction and capacity retention, enhancing the cycle performance at 4.6 V or 70 °C.

Furtherly, Liu et al. have introduced the 3-(trifluoromethyl) phenyl isocyanate (3-TPIC) into carbonate-based electrolytes, where the cleavage of the C−F bonds in the $-CF_3$ groups of the additive is facilitated by the polar −NCO groups [107]. This process results in the generation of more LiF. The additive groups can interact with each other, forming a heterogeneous structure on the surface of LCO with polar amide groups and the coexistence of Li_3N/LiF. In this structure, the lone pair electrons of O atoms in the amide groups can facilitate the Li^+ ions desolvation, thus accelerating the rate performance. XPS studies and DFT/MD calculations further indicate that the enrichment of Li_3N at the top of the CEI, coupled with the enrichment of LiF at the bottom, can favor the induction of Li^+ transport from top to bottom in the CEI film, thereby inducing uniform Li^+ transport dynamics. Zhang et al. have added the impure mixtures of LiDFBP containing 40wt% LiOTFP to the carbonate-based electrolytes, to construct a double layer CEI on LCO surface. Specifically, the outer CEI film is enriched in characteristic compounds such as LiF, P-B, and P-F, and the inner Co_3O_4 phase (2 nm), which further suppress the phase transition of LCO and Co dissolution.

Fu et al. added the potassium selenocyanate (KSeCN) in the carbonate (EC/DEC) electrolytes (Fig. 10c) [108]. The −C≡N group in KSeCN has lone pair electrons and can be easily coordinated with Co^{4+}, forming a strong interaction with R-$C{\equiv}N^{\delta-}$-$Co^{(4+\delta)+}$. This interaction can delay the oxidation and leaching of transition metal ions. The -Se in additive can be easily combined with Li^+, forming a protective CEI layer on the cathode and anode surfaces containing Se. Furtherly, Yang et al. have achieved the in-situ polymerization of a robust CEI on the cathodes (LCO and NCM) by adding aluminum isopropoxide (AIP) to commercial electrolytes [109]. The *in-situ* formed polymer CEI with strong Al−O bonds ensures a stable CEI. Furtherly, the organic-inorganic composite CEI with polycarbonate, Al_2O_3, and AlF_3 components plays a significant role on inhibiting the TMs dissolution and electrolyte decomposition.

In addition to adding additives to traditional carbonate-based electrolytes, researchers have innovatively modulated the solvents of electrolytes to meet the stability of electrolytes at higher voltage or other harsher conditions, such as high and low-temperature conditions. Zhang et al. have designed a fully fluorinated electrolyte (1 $mol \cdot L^{-1}$ $LiPF_6$ in fluoroethylene carbonate/methyl (2,2,2-trifluoroethyl) carbonate/1,1,2,2-tetrafluoroethyl-2,2,3,3-tetrafluoropropylether (FEC/FEMC/TTE) [denoted as AFE] + 2wt% tris(trimethylsilyl)borate (TMSB) [denoted as AFTB]) [110]. Comprehensive TEM, TOF-SIMS, and XPS results have confirmed the formation of a robust and inorganic-rich CEI on the LCO surface, consisting of B-, Si- compounds, and F-rich inorganic components. Liu et al. have added the iso-butyl formate (IF) as an anti-freezing agent to a fluorine-sulfur electrolyte to design an electrolyte that can be used in the extremely cold regions (Fig. 10d) [111]. The designed electrolyte presented an ultra-low melting point (−132 °C), ultra-low viscosity (0.3 Pa·s), and a high Li^+ concentration (1.40×10^{-10} $mol \cdot s^{-1}$), achieving excellent cycling performance at −70 °C. The electrolyte constructs a stable LiF-rich CEI on the LCO surface. Jiang et al. have replaced ester-based electrolytes with cyclic ethers, specifically 1,3-dioxolane (DOL), to design LCO batteries that can be operated in extremely low temperatures (Fig. 10e) [112]. However, due to its tendency to be polymerized in the presence of inorganic lithium salts and trace water, the authors used trimethylsilyl isocyanate (Si-NCO) as a water scavenger to eliminate water through nucleophilic addition. This strategy achieves an *in-situ* formed robust CEI through polymerization, with strong Al−O bonds, ensuring stable CEI. Additionally, the organic-inorganic composite CEI with polycarbonate, Al_2O_3, and AlF_3 components inhibited TM-ion dissolution and electrolyte decomposition.

Whether from the perspective of the material or electrolyte engineering, the mechanism is to regulate the electrochemical reactions on the surface of LCO, thereby achieving the effective construction of CEI during the cycling process. Surface regulation of LCO, such as coating, may undergo an *in-situ* transformation into customized CEI. Electrolyte engineering, on the other hand, involves controlling the electrolyte decomposition pathways and promoting the growth of specific CEI on the surface of LCO. Both approaches share the same goal and can be used in combination. However, due to the diversity of combinations and the uncertainty of electrochemical reactions arising from different operating conditions, the mechanism of interplay needs to be individually analyzed in specific situations [113]. For example, Fan et al. coated Li_3AlF_6 on LCO, simultaneously designing a highly compatible fluorinated electrolyte to jointly achieve high stability in LCO [68]. The synergistic effect of the two resulted in the formation of more $Li_xF_yPO_x$, which is considered to have better interface stabilization capabilities. Combining surface modification with the development of new electrolyte formulations can effectively passivate electrodes.

5. Conclusions and prospects

In summary, we have systematically reviewed the capacity decay issues and the related surface modulations for developing more advanced LCO cathodes. Based on the above reviews, some prospects for the future research and development of LCO materials are as follows:

(i) Since the current synthesis of the high-voltage LCO is high-cost, time-consuming, and laborious, more researches need to be conducted to explore low-cost and high-quality manufacturing procedure of the high-voltage LCO.

(ii) Researchers need to focus on developing some specific LCO products to meet various requirements in some extreme conditions, such as high-rate discharging and/or charging, high-temperature, and low-temperature conditions, etc.

(iii) To achieve the goal of developing LCO/Li full batteries having a cut-off voltage of 4.55 V or realizing a highly reversible capacity of 220 $mAh \cdot g^{-1}$ of LCO seems to be a very difficult task. More fundamental research works need to be done to reveal the mechanism of stabilizing the layered structure of LCO upon the highly delithiated state.

Acknowledgements

This work is financially supported by the National Natural Science Foundation of China (No. 52102201, No. 52102200), and the Basic and Applied Basic Research Foundation of Guangdong Province (No. 2021B1515130002).

References

[1] Lin C, Li J Y, Yin Z W, Huang W Y, Zhao Q H, Weng Q S, Liu Q, Sun J L, Chen G H, Pan F. Structural understanding for high-voltage stabilization of lithium cobalt oxide[J]. Adv. Mater. 2023: 2307404.

[2] Ren H Y, Zhao W G, Yi H C, Chen Z F, Ji H C, Jun Q, Ding W Y, Li Z J, Shang M J, Fang J J, Li K, Zhang M J, Li S N, Zhao Q H, Pan F. One-step sintering synthesis achieving multiple structure modulations for high-voltage $LiCoO_2$[J]. Adv. Funct. Mater., 2023, 33(38): 2302622.

[3] Lyu Y C, Wu X, Wang K, Feng Z J, Cheng T, Liu Y, Wang M, Chen R M, Xu L M, Zhou J J, Lu Y H, Guo B K. An overview on the advances of $LiCoO_2$ cathodes for lithium-ion batteries[J]. Adv. Energy Mater., 2021, 11(2): 2000982.

[4] Yu X R, Hu X L. Interface engineering by gelling sulfolane for durable and safe Li/$LiCoO_2$ batteries in wide temperature range[J]. Sci. China-Mater., 2022, 65(11): 2967−2974.

[5] Liu Y T, Wang L, Liu S, Li G R, Gao X P. Constructing high gravimetric and volumetric capacity sulfur cathode with $LiCoO_2$ nanofibers as carbon-free sulfur host for lithium-sulfur battery[J]. Sci. China-Mater., 2021, 64(6): 1343−1354.

[6] Konar R, Maiti S, Shpigel N, Aurbach D. Reviewing failure mechanisms and modification strategies in stabilizing high-voltage $LiCoO_2$ cathodes beyond 4.55v[J]. Energy Stor. Mater., 2023, 63: 103001.

[7] Qin R Z, Ding S X, Hou C X, Liu L L, Wang Y T, Zhao W G, Yao L, Shao Y L, Zou R Q, Zhao Q H, Li S N, Pan F. Modulating the proton-conducting lanes in spinel $ZnMn_2O_4$ through off-stoichiometry[J]. Adv. Energy Mater., 2023, 13(20): 2203915.

[8] Qian H M, Ren H Q, Zhang Y, He X F, Li W B, Wang J J, Hu J H, Yang H, Sari H MK, Chen Y, Li X F. Surface doping vs. Bulk doping of cathode materials for lithium-ion batteries: a review[J]. Electrochem. Energy Rev., 2022, 5(4): 2.

[9] Huang W Y, Zhao Q, Zhang M J, Xu S Y, Xue H Y, Zhu C, Fang J J, Zhao W G, Ren G X, Qin R Z, Zhao Q H, Chen H B, Pan F. Surface design with cation and anion dual gradient stabilizes high-voltage $LiCoO_2$[J]. Adv. Energy Mater., 2022, 12(20): 2200813.

[10] Zhang S D, Qi M Y, Guo S J, Sun Y G, Tan X X, Ma P Z, Li J Y, Yuan R Z, Cao A M, Wan L J. Advancing to 4.6 v review and prospect in developing high-energy-density $LiCoO_2$ cathode for lithium-ion batteries[J]. Small Methods, 2022, 6(5): 2200148.

[11] Xu S Y, Tan X H, Ding W Y, Ren W J, Zhao Q, Huang W Y, Liu J J, Qi R, Zhang Y X, Yang J C, Zuo C J, Ji H C, Ren H Y, Cao B, Xue H Y, Gao Z H, Yi H C, Zhao W G, Xiao Y G, Zhao Q H, Zhang M J, Pan F. Promoting surface electric conductivity for high-rate $LiCoO_2$[J]. Angew. Chem. Int. Ed., 2023, 62(10): e202218595.

[12] Wu Q, Zhang B, Lu Y Y. Progress and perspective of high-voltage lithium cobalt oxide in lithium-ion batteries[J]. J. Energy Chem., 2022, 74: 283−308.

[13] Zhang N, Wang B, Jin F, Chen Y, Jiang Y P, Bao C Y, Tian J Y, Wang J Y, Xu R Y, Li Y H, Lv Q, Ren H Z, Wang D L, Liu H K, Dou S X, Hong X. Modified cathode-electrolyte interphase toward high-performance batteries [J]. Cell Rep. Phys. Sci., 2022, 3(12): 101197.

[14] Liang L W, Zhang W H, Zhao F, Denis D K, Zaman F U, Hou L R, Yuan C Z. Surface/interface structure degradation of Ni-rich layered oxide cathodes toward lithium-ion batteries: fundamental mechanisms and remedying strategies[J]. Adv. Mater. Interfaces, 2020, 7(3): 1901749.

[15] Li Z J, Yi H C, Ding W Y, Ren H Y, Du Y H, Shang M J, Zhao W G, Chen H, Zhou L, Lin H, Zhao Q H, Pan F. Revealing the accelerated capacity decay of a high-voltage $LiCoO_2$ upon harsh charging procedure[J]. Adv. Funct. Mater., 2023, 34(14): 2312837.

[16] Zhang J Y, Gai J J, Song K M, Chen W H. Advances in electrode/electrolyte interphase for sodium-ion batteries from half cells to full cells[J]. Cell Rep. Phys. Sci., 2022, 3(5): 100868.

[17] He W, Guo W B, Wu H L, Lin L, Liu Q, Han X, Xie Q S, Liu P F, Zheng H F, Wang L S, Yu X Q, Peng D L. Challenges and recent advances in high capacity Li-rich cathode materials for high energy density lithium-ion batteries[J]. Adv. Mater., 2021, 33(50): 2005937.

[18] Maleki Kheimeh Sari H, Li X. Controllable cathode-electrolyte interface of $Li[Ni_{0.8}Co_{0.1}Mn_{0.1}]O_2$ for lithium ion batteries: a review[J]. Adv. Energy Mater., 2019, 9(39): 1901597.

[19] Chen J K, Lin Z Y, Xiang W J, Wu B H, Zhang G G, Wen X Y, Che Y X, Ruan D G, Li W S, Chen M. Investigation of degradation mechanism of $LiCoO_2$/graphite batteries with multiscale characterization[J]. Electrochim. Acta, 2022, 436: 141374.

[20] Wu Z X, Zeng G F, Yin J H, Chiang C L, Zhang Q H, Zhang B D, Chen J K, Yan Y W, Tang Y L, Zhang H T, Zhou S Y, Wang Q S, Kuai X X, Lin Y G, Gu L, Qiao Y, Sun S G. Unveiling the evolution of $LiCoO_2$ beyond 4.6V [J]. ACS Energy Lett., 2023, 8(11): 4806−4817.

[21] Li S, Sun Y, Gao A, Zhang Q H, Lu X Y, Lu X. Sustainable $LiCoO_2$ by collective glide of CoO_6 slabs upon charge/discharge[J]. Proc. Natl. Acad. Sci., 2022, 119(20): e2120060119.

[22] Jiang Y Y, Qin C D, Yan P F, Sui M L. Origins of capacity and voltage fading of $LiCoO_2$ upon high voltage cycling[J]. J. Mater. Chem. A, 2019, 7(36): 20824−20831.

[23] Duffiet M, Blangero M, Cabelguen P E, Delmas C, Carlier D. Influence of the initial Li/Co ratio in $LiCoO_2$ on the high-voltage phase-transitions mechanisms[J]. J. Phys. Chem. Lett., 2018, 9(18): 5334−5338.

[24] Liu Q, Su X, Lei D, Qin Y, Wen J G, Guo F M, Wu Y MA, Rong Y C, Kou R H, Xiao X H, Aguesse F, Bareño J, Ren Y, Lu W Q, Li Y X. Approaching the capacity limit of lithium cobalt oxide in lithium ion batteries via lanthanum and aluminium doping[J]. Nat. Energy, 2018, 3(11): 936−943.

[25] Jiang Y Y, Yan P F, Yu M C, Li J M, Jiao H, Zhou B, Sui M L. Atomistic mechanism of cracking degradation at twin boundary of $LiCoO_2$[J]. Nano Energy, 2020, 78: 105364.

[26] Kim D, Hwang J, Byeon P, Kim W, Kang D G, Bae H B, Lee S G, Han S M, Lee J, Chung S Y. Direct probing of lattice-strain-induced oxygen release in $LiCoO_2$ and Li_2MnO_3 without electrochemical cycling[J]. Adv. Mater., 2023, 35(29): 2212098.

[27] Jena A, Lee P H, Pang W K, Hsiao K C, Peterson V K, Darwish T, Yepuri N, Wu S H, Chang H, Liu R S. Monitoring the phase evolution in $LiCoO_2$ electrodes during battery cycles using *in-situ* neutron diffraction technique [J]. J. Chin. Chem. Soc., 2020, 67(3): 344−352.

[28] Ding S X, Zhang M Z, Qin R Z, Fang J J, Ren H Y, Yi H C, Liu L L, Zhao W G, Li Y, Yao L, Li S N, Zhao Q H, Pan F. Oxygen-deficient β-Mno_2@graphene oxide cathode for high-rate and long-life aqueous zinc ion batteries[J]. Nanomicro Lett, 2021, 13(1): 173.

[29] Hitt A, Wang F, Li Z, Ge M, Zhang Y, Savsatli Y, Xiao X, Lee W K, Stephens R, Tang M. Nanotomographic observation and statistical analysis of overcharging induced cracks in $LiCoO_2$ single crystalline particles[J]. Energy Stor. Mater., 2022, 52: 320−328.

[30] Xu Y H, Hu E Y, Zhang K, Wang X L, Borzenets V, Sun Z H, Pianetta P, Yu X Q, Liu Y J, Yang X Q, Li H. *In situ* visualization of state-of-charge heterogeneity within a $LiCoO_2$ particle that evolves upon cycling at different rates[J]. ACS Energy Lett, 2017, 2(5): 1240−1245.

[31] Zhu Y M, Wu D J, Yang X M, Zeng L Y, Zhang J, Chen D L, Wang B, Gu M. Microscopic investigation of crack and strain of $LiCoO_2$ cathode cycled under high voltage[J]. Energy Stor. Mater., 2023, 60: 102828.

[32] Oh J, Lee S Y, Kim H, Ryu J, Gil B, Lee J, Kim M. Overcharge-induced phase heterogeneity and resultant twin-like layer deformation in lithium cobalt oxide cathode for lithium-ion batteries[J]. Adv. Sci., 2022, 9(32): 2203639.

[33] Yaqoob N, Mücke R, Guillon O, Kaghazchi P. Delithiation-induced oxygen vacancy formation increases microcracking of $LiCoO_2$ cathodes[J]. J. Power Sources, 2022, 533: 231316.

[34] He Y F, Wang L, Zhang B, Pham H, Xu H, Park J, He X M. Atomic-scale insight into the lattice volume plunge of Li_xCoO_2 upon deep delithiation[J]. Energy Advances, 2023, 2(1): 103−112.

[35] Hu E Y, Li Q H, Wang X L, Meng F Q, Liu J, Zhang J N, Page K, Xu W Q, Gu L, Xiao R J, Li H, Huang X J, Chen L Q, Yang W L, Yu X Q, Yang X Q. Oxygen-redox reactions in $LiCoO_2$ cathode without O−O bonding during charge-discharge[J]. Joule, 2021, 5(3): 720−736.

[36] Geng F S, Shen M, Hu B, Liu Y F, Zeng L C, Hu B W. Monitoring the evolution of local oxygen environments during $LiCoO_2$ charging via *ex situ* ^{17}O NMR[J]. Chem. Commun., 2019, 55(52): 7550−7553.

[37] Li C F, Zhao K, Liao X, Hu Z Y, Zhang L, Zhao Y, Mu S, Li Y, Li Y, Van Tendeloo G, Sun C. Interface cation migration kinetics induced oxygen release heterogeneity in layered lithium cathodes[J]. Energy Stor. Mater., 2021, 36: 115−122.

[38] Hu T, Dai F Z, Zhou G, Wang X, Xu S. Unraveling the dynamic correlations between transition metal migration and the oxygen dimer formation in the highly delithiated Li_xCoO_2 cathode[J]. J. Phys. Chem. Lett., 2023, 14(15): 3677−3684.

[39] Sun C L, Liao X B, Xia F J, Zhao Y, Zhang L, Mu S, Shi S, Li Y X, Peng H Y, Van Tendeloo G, Zhao K N, Wu J S. High-voltage cycling induced thermal vulnerability in $LiCoO_2$ cathode: cation loss and oxygen release driven by oxygen vacancy migration[J]. ACS Nano, 2020, 14(5): 6181−6190.

[40] Lu W, Zhang J S, Xu J J, Wu X D, Chen L W. *In situ* visualized cathode electrolyte interphase on $LiCoO_2$ in high voltage cycling[J]. ACS Appl. Mater. Interfaces, 2017, 9(22): 19313−19318.

[41] Rinkel B LD, Hall D S, Temprano I, Grey C P. Electrolyte oxidation pathways in lithium-ion batteries[J]. J. Am. Chem. Soc., 2020, 142(35): 15058−15074.

[42] Li J Y, Lin C, Weng M Y, Qiu Y, Chen P H, Yang K, Huang W Y, Hong Y X, Li J, Zhang M J, Dong C, Zhao W G, Xu Z, Wang X, Xu K, Sun J L, Pan F. Structural origin of the high-voltage instability of lithium cobalt oxide[J]. Nat. Nanotechnol., 2021, 16(5): 599−605.

[43] Takamatsu D, Koyama Y, Orikasa Y, Mori S, Nakatsutsumi T, Hirano T, Tanida H, Arai H, Uchimoto Y, Ogumi Z. First *in situ* observation of the $LiCoO_2$ electrode/electrolyte interface by total-reflection X-ray absorption spectroscopy[J]. Angew. Chem. Int. Ed., 2012, 51(46): 11597−11601.

[44] Kikkawa J, Terada S, Gunji A, Nagai T, Kurashima K, Kimoto K. Chemical states of overcharged $LiCoO_2$ particle surfaces and interiors observed using electron energy-loss spectroscopy[J]. J. Phys. Chem. C, 2015, 119(28): 15823−15830.

[45] Qin C D, Jiang Y Y, Yan P F, Sui M L. Revealing the minor Li-ion blocking effect of $LiCoO_2$ surface phase transition layer[J]. J. Power Sources, 2020, 460: 228126.

[46] Yano A, Shikano M, Ueda A, Sakaebe H, Ogumi Z. $LiCoO_2$ degradation behavior in the high-voltage phase transition region and improved reversibility with surface coating[J]. J. Electrochem. Soc., 2017, 164(1): A6116.

[47] Seong W M, Yoon K, Lee M H, Jung S K, Kang K. Unveiling the intrinsic cycle reversibility of a $LiCoO_2$ electrode at 4.8 V cutoff voltage through subtractive surface modification for lithium-ion batteries[J]. Nano Lett., 2019, 19(1): 29−37.

[48] Li S, Li K L, Zheng J Y, Zhang Q H, Wei B, Lu X. Structural distortion-induced charge gradient distribution of Co ions in delithiated $LiCoO_2$ cathode[J]. J. Phys. Chem. Lett., 2019, 10(24): 7537−7546.

[49] Hirooka M, Sekiya T, Omomo Y, Yamada M, Katayama H, Okumura T, Yamada Y, Ariyoshi K. Degradation mechanism of $LiCoO_2$ under float charge conditions and high temperatures[J]. Electrochim. Acta, 2019, 320: 134596.

[50] Wang K, Zhang Z, Ding Y, Cheng S, Xiao B, Sui M, Yan P. Surface facet dependent cycling stability of layered cathodes[J]. Adv. Funct. Mater., 2023, 33(37): 2302023.

[51] Zhang J N, Li Q, Wang Y, Zheng J, Yu X, Li H. Dynamic evolution of cathode electrolyte interphase (CEI) on high voltage $LiCoO_2$ cathode and its interaction with Li anode [J]. Energy Stor. Mater., 2018, 14: 1−7.

[52] Cho J, Kim Y J, Park B. Novel $LiCoO_2$ cathode material with Al_2O_3 coating for a Li ion cell[J]. Chem. Mater., 2000, 12(12): 3788−3791.
[53] Cho J, Kim Y J, Park B. $LiCoO_2$ cathode material that does not show a phase transition from hexagonal to monoclinic phase[J]. J. Electrochem. Soc., 2001, 148(10): A1110.
[54] Jian Z L, Wang W T, Wang M Y, Wang Y, AuYeung N, Liu M, Feng Z X. Al_2O_3 coated $LiCoO_2$ as cathode for high-capacity and long-cycling Li-ion batteries[J]. Chin. Chem. Lett., 2018, 29(12): 1768−1772.
[55] Wang Z X, Wu C A, Liu L J, Wu F, Chen L Q, Huang X J. Electrochemical evaluation and structural characterization of commercial $LiCoO_2$ surfaces modified with MgO for lithium-ion batteries[J]. J. Electrochem. Soc., 2002, 149(4): A466.
[56] Shim J H, Lee S, Park S S. Effects of MgO coating on the structural and electrochemical characteristics of $LiCoO_2$ as cathode materials for lithium ion battery[J]. Chem. Mater., 2014, 26(8): 2537−2543.
[57] Yamamoto K, Orikasa Y, Takamatsu D, Koyama Y, Mori S, Masese T, Mori T, Minato T, Tanida H, Uruga T, Ogumi Z, Uchimoto Y. Stabilization of the electronic structure at the cathode/electrolyte interface via MgO ultra-thin layer during lithium-ions insertion/extraction[J]. Electrochemistry, 2014, 82(10): 891−896.
[58] Han B, Paulauskas T, Key B, Peebles C, Park J S, Klie R F, Vaughey J T, Dogan F. Understanding the role of temperature and cathode composition on interface and bulk: optimizing aluminum oxide coatings for Li-ion cathodes[J]. ACS Appl. Mater. Interfaces, 2017, 9(17): 14769−14778.
[59] Xiao B, Tang Q C, Dai X Y, Wu F Z, Chen H J, Li J Z, Mai Y, Gu Y J. Enhanced interfacial kinetics and high rate performance of $LiCoO_2$ thin-film electrodes by Al doping and *in situ* Al_2O_3 coating[J]. ACS Omega, 2022, 7(35): 31597−31606.
[60] Kim A, Won Y, Woo K, Kim C H, Moon J. Highly transparent low resistance ZnO/Ag nanowire/ZnO composite electrode for thin film solar cells[J]. ACS Nano, 2013, 7(2): 1081−1091.
[61] Fu Q Y, Hao S, Shen B, Duan X B, Na H C. Preparation and optical-electrical properties of Al-doped ZnO films[J]. Res. Chem. Intermed., 2013, 39(2): 527−536.
[62] Shen B, Zuo P J, Li Q, He X S, Yin G P, Ma Y L, Cheng X Q, Du C Y, Gao Y Z. Lithium cobalt oxides functionalized by conductive Al-doped ZnO coating as cathode for high-performance lithium ion batteries[J]. Electrochim. Acta, 2017, 224: 96−104.
[63] Zhou A J, Lu Y T, Wang Q J, Xu J, Wang W H, Dai X Y, Li J Z. Sputtering TiO_2 on $LiCoO_2$ composite electrodes as a simple and effective coating to enhance high-voltage cathode performance[J]. J. Power Sources, 2017, 346: 24−30.
[64] Yang Q, Huang J, Li Y J, Wang Y, Qiu J L, Zhang J N, Yu H G, Yu X Q, Li H, Chen L Q. Surface-protected $LiCoO_2$ with ultrathin solid oxide electrolyte film for high-voltage lithium ion batteries and lithium polymer batteries[J]. J. Power Sources, 2018, 388: 65−70.
[65] Li Z, Li A, Zhang H, Ning F, Li W, Zangiabadi A, Cheng Q, Borovilas J J, Chen Y, Zhang H, Xiao X, Ouyang C, Huang X, Lee W K, Ge M, Chu Y S, Chuan X, Yang Y. Multi-scale stabilization of high-voltage $LiCoO_2$ enabled by nanoscale solid electrolyte coating[J]. Energy Stor. Mater., 2020, 29: 71−77.
[66] Wei J, Ji Y X, Liang D, Chen B, Jiang C, Li X T. Anticorrosive nanosized LiF thin film coating for achieving long-cycling stability of $LiCoO_2$ at high voltages[J]. Ceram. Int., 2022, 48(7): 10288−10298.
[67] Mao S L, Shen Z Y, Zhang W D, Wu Q, Wang Z Y, Lu Y Y. Outside-in nanostructure fabricated on $LiCoO_2$ surface for high-voltage lithium-ion batteries[J]. Adv. Sci., 2022, 9(11): 2104841.
[68] Fan T, Kai W, Harika V K, Liu C, Nimkar A, Leifer N, Maiti S, Grinblat J, Tsubery M N, Liu X, Wang M, Xu L, Lu Y, Min Y, Shpigel N, Aurbach D. Operating highly stable $LiCoO_2$ cathodes up to 4.6 V by using an effective integration of surface engineering and electrolyte solutions selection[J]. Adv. Funct. Mater., 2022, 32(33): 2204972.
[69] Wang X, Wu Q, Li S Y, Tong Z M, Wang D, Zhuang H LL, Wang X Y, Lu Y Y. Lithium-aluminum-phosphate coating enables stable 4.6 V cycling performance of $LiCoO_2$ at room temperature and beyond[J]. Energy Stor. Mater., 2021, 37: 67−76.
[70] Ye B, Cai M Z, Xie M, Dong H, Dong W J, Huang F Q. Constructing robust cathode/electrolyte interphase for ultrastable 4.6 V $LiCoO_2$ under -25 °C[J]. ACS Appl Mater Interfaces, 2022, 14(17): 19561−19568.
[71] Yang X R, Wang C W, Yan P F, Jiao T P, Hao J L, Jiang Y Y, Ren F C, Zhang W G, Zheng J M, Cheng Y, Wang X S, Yang W, Zhu J P, Pan S Y, Lin M, Zeng L Y, Gong Z L, Li J T, Yang Y. Pushing lithium cobalt oxides to 4.7 V by lattice-matched interfacial engineering[J]. Adv. Energy Mater., 2022, 12(23): 2200197.
[72] Zhuang Z F, Wang J X, Jia K, Ji G L, Ma J, Han Z Y, Piao Z H, Gao R H, Ji H C, Zhong X W, Zhou G M, Cheng H M. Ultrahigh-voltage $LiCoO_2$ at 4.7 V by interface stabilization and band structure modification[J]. Adv. Mater., 2023, 35(22): 2212059.
[73] Dong W J, Ye B, Cai M Z, Bai Y Z, Xie M, Sun X Z, Lv Z R, Huang F Q. Superwettable high-voltage $LiCoO_2$ for low-temperature lithium ion batteries[J]. ACS Energy Lett., 2023, 8(2): 881−888.
[74] Pu W, Meng Y, Wang Y J, Ge Y C, Li X P, Wang P F, Zhang Z K, Guo Y, Xiao D. Investigation of the $LiBH_4$ modification effect on cycling stability and high-rate capacity of $LiCoO_2$ cathodes[J]. ACS Appl. Energy Mater., 2021, 4(7): 6933−6941.
[75] Chen J, Chen H Y, Zhang S, Dai A, Li T Y, Mei Y, Ni L S, Gao X, Deng W T, Yu L, Zou G Q, Hou H S, Dahbi M, Xu W Q, Wen J G, Alami J, Liu T C, Amine K, Ji X B. Structure/interface coupling effect for high-voltage $LiCoO_2$ cathodes[J]. Adv. Mater., 2022, 34(42): 2204845.
[76] Zhu Z, Wang H, Li Y, Gao R, Xiao X H, Yu Q P, Wang C, Waluyo I, Ding J X, Hunt A, Li J. A surface Se-substituted $LiCo[O_{2-\delta}Se_\delta]$ cathode with ultrastable high-voltage cycling in pouch full-cells[J]. Adv. Mater., 2020, 32(50): 2005182.
[77] Fu A, Zhang Z F, Lin J D, Zou Y, Qin C D, Xu C J, Yan P F, Zhou K, Hao J L, Yang X R, Cheng Y, Wu D Y, Yang Y, Wang M S, Zheng J M. Highly stable operation of $LiCoO_2$ at cut-off $\geq$ 4.6 V enabled by synergistic structural and interfacial manipulation[J]. Energy Stor. Mater., 2022, 46: 406−416.
[78] Seong W M, Cho K H, Park J W, Park H, Eum D, Lee M H, Kim I SS, Lim J, Kang K. Controlling residual lithium in high-nickel (>90 %) lithium layered oxides for cathodes in lithium-ion batteries[J]. Angew. Chem. Int. Ed., 2020, 59(42): 18662−18669.
[79] Kim J, Lee J, Bae C, Kang B. Sublimation-induced gas-reacting process for high-energy-density Ni-rich electrode materials[J]. ACS Appl. Mater. Interfaces, 2020, 12(10): 11745−11752.
[80] Du F H, Fan Z X, Ding L, Wang Y, Shi W J, Zhang J, Qu H Y, Yu X X, Chen Y L, Zheng J W. Surface engineering based on element interdiffusion and interfacial reactions to boost the performance of $LiCoO_2$ cathode material[J]. Chem. Eng. J., 2023, 474: 145952.

[81] Qian J W, Liu L, Yang J X, Li S Y, Wang X, Zhuang H LL L, Lu Y Y. Electrochemical surface passivation of $LiCoO_2$ particles at ultrahigh voltage and its applications in lithium-based batteries[J]. Nat. Commun., 2018, 9(1): 4918.

[82] Li Z J, Yi H C, Ren H Y, Fang J J, Du Y H, Zhao W G, Chen H, Zhao Q H, Pan F. Multiple surface optimizations for a highly durable $LiCoO_2$ beyond 4.6 V[J]. Adv. Funct. Mater., 2023, 33(46): 2307913.

[83] Wang Y, Zhang Q H, Xue Z C, Yang L F, Wang J Y, Meng F Q, Li Q H, Pan H Y, Zhang J N, Jiang Z, Yang W L, Yu X Q, Gu L, Li H. An *in situ* formed surface coating layer enabling $LiCoO_2$ with stable 4.6 V high-voltage cycle performances[J]. Adv. Energy Mater., 2020, 10(28): 2001413.

[84] Li Y, Zan M W, Chen P H, Huang Y L, Xu X L, Zhang C Z, Cai Z Y, Yu X Q, Li H. Facile solid-state synthesis to *in situ* generate a composite coating layer composed of spinel-structural compounds and Li_3PO_4 for stable cycling of $LiCoO_2$ at 4.6 V[J]. ACS Appl. Mater. Interfaces, 2023, 15(44): 51262−51273.

[85] Li M Y, Bai F Y, Yao Q, Wang H C, Li P. Double function-layers construction strategy promotes the cycling stability of $LiCoO_2$ under high temperature and high voltage[J]. Electrochim. Acta, 2023, 449: 142197.

[86] Tan X H, Mao D D, Zhao T Q, Zhang Y X, Song L T, Fan Z W, Liu G Y, Wang H F, Chu W G. Long-term highly stable high-voltage $LiCoO_2$ synthesized via a solid sulfur-assisted one-pot approach[J]. Small, 2022, 18(26): 2202143.

[87] Tan X H, Zhao T Q, Song L T, Mao D D, Zhang Y X, Fan Z W, Wang H F, Chu W G. Simultaneous near-surface trace doping and surface modifications by gas-solid reactions during one-pot synthesis enable stable high-voltage performance of $LiCoO_2$[J]. Adv. Energy Mater., 2022, 12(30): 2200008.

[88] Zhang Q Y, Ma J L, Mei L, Liu J, Li Z Y, Li J, Zeng Z Y. *In situ* tem visualization of LiF nanosheet formation on the cathode-electrolyte interphase (CEI) in liquid-electrolyte lithium-ion batteries[J]. Matter, 2022, 5(4): 1235−1250.

[89] Yan Y W, Zheng Y C, Zhang H T, Chen J K, Zeng G F, Wang L L, Zhang B D, Zhou S Y, Tang Y L, Fu A, Zheng L R, Huang H, Zou Y, Wang C W, Kuai X X, Sun Y, Qiao Y, Sun S G. Blending layered cathode with olivine: an economic strategy for enhancing the structural and thermal stability of 4.65 V $LiCoO_2$[J]. Adv. Funct. Mater., 2023, 33(43): 2304496.

[90] Liu J X, Wang J Q, Ni Y X, Liu J D, Zhang Y D, Lu Y, Yan Z H, Zhang K, Zhao Q, Cheng F Y, Chen J. Tuning interphase chemistry to stabilize high-voltage $LiCoO_2$ cathode material via spinel coating[J]. Angew. Chem. Int. Ed., 2022, 61(35): e202207000.

[91] Wang L L, Ma J, Wang C, Yu X R, Liu R, Jiang F, Sun X W, Du A B, Zhou X H, Cui G L. A novel bifunctional self-stabilized strategy enabling 4.6 V $LiCoO_2$ with excellent long-term cyclability and high-rate capability[J]. Adv. Sci., 2019, 6(12): 1900355.

[92] Zhang W, Cheng F Y, Chang M, Xu Y, Li Y Y, Sun S X, Wang L, Xu L M, Li Q, Fang C, Wang M, Lu Y H, Han J T, Huang Y H. Surface-interspersed nanoparticles induced cathode-electrolyte interphase enabling stable cycling of high-voltage $LiCoO_2$[J]. Nano Energy, 2024, 119: 109031.

[93] Wang F M, Chemere E B, Chien W C, Chen C L, Hsu C C, Yeh N H, Wu Y S, Khotimah C, Guji K W, Merinda L. In situ Co−O bond reinforcement of the artificial cathode electrolyte interphase in highly delithiated $LiCoO_2$ for high-energy-density applications[J]. ACS Appl. Mater. Interfaces, 2021, 13(39): 46703−46716.

[94] Zhou H, Izumi J, Asano S, Ito K, Watanabe K, Suzuki K, Nemoto F, Yamada N L, Aso K, Oshima Y, Kanno R, Hirayama M. Fast lithium intercalation mechanism on surface-modified cathodes for lithium-ion batteries[J]. Adv. Energy Mater., 2023, 13(44): 2370183.

[95] Zhang Y, Katayama Y, Tatara R, Giordano L, Yu Y, Fraggedakis D, Sun J G, Maglia F, Jung R, Bazant M Z, Shao-Horn Y. Revealing electrolyte oxidation via carbonate dehydrogenation on Ni-based oxides in Li-ion batteries by *in situ* fourier transform infrared spectroscopy[J]. Energy Environ. Sci., 2020, 13(1): 183−199.

[96] Fan X L, Wang C S. High-voltage liquid electrolytes for Li batteries: progress and perspectives[J]. Chem. Soc. Rev., 2021, 50(18): 10486−10566.

[97] Freiberg A TS, Sicklinger J, Solchenbach S, Gasteiger H A. Li_2CO_3 decomposition in Li-ion batteries induced by the electrochemical oxidation of the electrolyte and of electrolyte impurities[J]. Electrochim. Acta, 2020, 346: 136271.

[98] Shi C G, Shen C H, Peng X X, Luo C X, Shen L F, Sheng W J, Fan J J, Wang Q, Zhang S J, Xu B B, Xian J J, Wei Y M, Huang L, Li J T, Sun S G. A special enabler for boosting cyclic life and rate capability of $LiNi_{0.8}Co_{0.1}Mn_{0.1}O_2$: green and simple additive[J]. Nano Energy, 2019, 65: 104084.

[99] Bizuneh G G, Zhu C L, Huang J D, Wang H P, Qi S H, Wang Z S, Wu D X, Ma J M. Constructing highly Li^+ conductive electrode electrolyte interphases for 4.6 V Li||$LiCoO_2$ batteries via electrolyte additive engineering [J]. Small Methods, 2023, 7(9): 2300079.

[100] Solchenbach S, Metzger M, Egawa M, Beyer H, Gasteiger H A. Quantification of PF_5 and POF_3 from side reactions of $LiPF_6$ in Li-ion batteries[J]. J. Electrochem. Soc., 2018, 165(13): A3022.

[101] Yan Y W, Weng S T, Fu A, Zhang H T, Chen J K, Zheng Q Z, Zhang B D, Zhou S Y, Yan H, Wang C AW, Tang Y L, Luo H Y, Mao B W, Zheng J W, Wang X F, Qiao Y, Yang Y, Sun S G. Tailoring electrolyte dehydrogenation with trace additives: stabilizing the $LiCoO_2$ cathode beyond 4.6 V[J]. ACS Energy Lett., 2022, 7(8): 2677−2684.

[102] Tebbe J L, Fuerst T F, Musgrave C B. Degradation of ethylene carbonate electrolytes of lithium ion batteries via ring opening activated by $LiCoO_2$ cathode surfaces and electrolyte species[J]. ACS Appl. Mater. Interfaces, 2016, 8(40): 26664−26674.

[103] Guo K L, Zhu C L, Wang H P, Qi S H, Huang J D, Wu D X, Ma J M. Conductive Li^+ moieties-rich cathode electrolyte interphase with electrolyte additive for 4.6 V well-cycled Li||$LiCoO_2$ batteries[J]. Adv. Energy Mater., 2023, 13(20): 2204272.

[104] Xing L D, Li W S, Xu M Q, Li T T, Zhou L. The reductive mechanism of ethylene sulfite as solid electrolyte interphase film-forming additive for lithium ion battery[J]. J. Power Sources, 2011, 196(16): 7044−7047.

[105] Yang X R, Lin M, Zheng G R, Wu J, Wang X S, Ren F C, Zhang W G, Liao Y, Zhao W M, Zhang Z R, Xu N B, Yang W L, Yang Y. Enabling stable high-voltage $LiCoO_2$ operation by using synergetic interfacial modification strategy[J]. Adv. Funct. Mater., 2020, 30(43): 2004664.

[106] Sun Z Y, Li F K, Ding J Y, Lin Z Y, Xu M Q, Zhu M, Liu J. High-voltage and high-temperature $LiCoO_2$ operation via the electrolyte additive of electron-defect boron compounds[J]. ACS Energy Lett., 2023, 8(6): 2478−2487.

[107] Liu J D, Wu M G, Li X, Wu D X, Wang H P, Huang J D, Ma J M. Amide-functional, Li_3N/LiF-rich heterostructured electrode eectrolyte interphases for 4.6 V Li||$LiCoO_2$ batteries[J]. Adv. Energy Mater., 2023, 13(15): 2300084.

[108] Fu A, Lin J D, Zhang Z F, Xu C J, Zou Y, Liu C Y, Yan P F, Wu D Y, Yang Y, Zheng J M. Synergistical stabilization of Li metal anodes and $LiCoO_2$ cathodes in high-voltage Li||$LiCoO_2$ batteries by potassium selenocyanate (KSeCN) additive[J]. ACS Energy Lett., 2022, 7(4): 1364−1373.

[109] Yang J X, Liu X, Wang Y A, Zhou X W, Weng L T, Liu Y Z, Ren Y, Zhao C, Dahbi M, Alami J, Ei-Hady D A, Xu G L, Amine K, Shao M H. Electrolytes polymerization-induced cathode-electrolyte-interphase for high voltage lithium-ion batteries[J]. Adv. Energy Mater., 2021, 11(39): 2101956.
[110] Zhang J X, Wang P F, Bai P X, Wan H L, Liu S F, Hou S, Pu X J, Xia J L, Zhang W R, Wang Z Y, Nan B, Zhang X Y, Xu J J, Wang C S. Interfacial design for a 4.6 V high-voltage single-crystalline $LiCoO_2$ cathode[J]. Adv. Mater., 2022, 34(8): 2108353.
[111] Liu J P, Yuan B T, He N AD, Dong L W, Chen D J, Zhong S J, Ji Y P, Han J C, Yang C H, Liu Y P, He W D. Reconstruction of LiF-rich interphases through an anti-freezing electrolyte for ultralow-temperature $LiCoO_2$ batteries[J]. Energy Environ. Sci., 2023, 16(3): 1024−1034.
[112] Jiang H Z, Yang C, Chen M, Liu X W, Yin L M, You Y, Lu J. Electrophilically trapping water for preventing polymerization of cyclic ether towards low-temperature Li metal battery[J]. Angew. Chem. Int. Ed., 2023, 62(14): e202300238.
[113] Zhang J Y, Yan Y L, Wang X, Cui Y Y, Zhang Z F, Wang S, Xie Z K, Yan P F, Chen W H. Bridging multiscale interfaces for developing ionically conductive high-voltage iron sulfate-containing sodium-based battery positive electrodes[J]. Nat. Commun., 2023, 14(1): 3701.

高电压 $LiCoO_2$ 的表面结构与性能：回顾与展望

方建军 [a,b]，杜宇豪 [a]，李子健 [a]，樊文光 [a,*]，任恒宇 [a]，易浩聪 [a]，赵庆贺 [a,*]，潘锋 [a,*]
[a] 北京大学深圳研究生院新材料学院，中国 深圳 518055
[b] 乾途电池科技有限公司，中国 东莞 523808

摘要

近年来，高电压 $LiCoO_2$（LCO）正极的研发成为学术界和工业界广泛关注的焦点。研究表明，解决表面问题是提升高电压 LCO 性能的最有效途径。本综述系统回顾了高电压 LCO 所面临的问题，包括相变和裂纹的生成、与氧氧化还原相关的问题以及副反应，以及表面结构的退化。接着，我们深入阐述了表面调制，以及表面调制与电解质调制之间的相互作用。最后，我们展望了更先进的 LCO 正极的发展前景，包括低成本高质量的制造，设计适用于极端条件（如高温、高速充电、低温等）的 LCO 正极，并实现约 220 $mAh·g^{-1}$ 的稳定容量释放。我们期望这项工作能为未来推动高电压 LCO 的发展和应用提供参考。

关键词： $LiCoO_2$；界面结构；相转变；表面修饰；正极电解质界面